Trimodal Characteristics of Tropical Convection

RICHARD H. JOHNSON, THOMAS M. RICKENBACH,* STEVEN A. RUTLEDGE,
PAUL E. CIESIELSKI, AND WAYNE H. SCHUBERT

Department of Atmospheric Science, Colorado State University, Fort Collins, Colorado

ABSTRACT

It has long been known that trade wind cumulus and deep cumulonimbus represent primary components of the broad spectrum of cumulus clouds in the Tropics, which has led to the concept of a bimodal distribution of tropical clouds. However, recent analyses of shipboard radar data from Tropical Ocean Global Atmosphere Coupled Ocean–Atmosphere Response Experiment (COARE) provide evidence of abundant populations of a third cloud type, *cumulus congestus*. Congestus clouds constitute over half the precipitating convective clouds in COARE and contribute over one-quarter of the total convective rainfall. Global Atmospheric Research Program Atlantic Tropical Experiment studies reveal a similar midlevel peak in the distribution of radar-echo tops. These findings lead to the conclusion that *shallow cumulus, congestus,* and *cumulonimbus* are all prominent tropical cumulus cloud types. They are associated with trimodal distributions of divergence, cloud detrainment, and fractional cloudiness in the Tropics.

The peaks in the distributions of radar-echo tops for these three cloud types are in close proximity to prominent stable layers that exist over the Pacific warm pool and the tropical eastern Atlantic: near 2 km (the trade stable layer), ~5 km (near 0°C), and ~15–16 km (the tropopause). These stable layers are inferred to inhibit cloud growth and promote cloud detrainment. The 0°C stable layer can produce detrainment from cumulonimbi (attendant shelf clouds) and help retard the growth of precipitation-laden and strongly entraining congestus clouds. Moreover, restriction of growth of congestus clouds to just above the 0°C level limits further enhancement of cloud buoyancy through glaciation.

The three cloud types are found to vary significantly during COARE on the timescale of the 30–60-day intraseasonal oscillation. The specific roles of clouds of the congestus variety in the general circulation are not yet clear, but some (the shallower ones) contribute to moistening and preconditioning the atmosphere for deep convection; others (the deeper ones) contribute an important fraction of the total tropical rainfall, and both likely produce many midlevel clouds, thereby modulating the radiative heating of the tropical atmosphere.

1. Introduction

a. Early observations of tropical convection

The Tropics harbor a spectacular variety of clouds. However, two types are generally regarded as dominant: (shallow) trade wind cumulus and deep cumulonimbus. Both cloud types can appear in isolation or in groups. For example, shallow cumulus clouds are frequently organized into bands, streets, or patches (Woodcock 1940; Malkus and Riehl 1964; Kuettner 1959, 1971; LeMone and Meitin 1984) or, in light-wind conditions, into Bénard cells (Krueger and Fritz 1961; Agee 1984).

* Current affiliation: Joint Center for Earth Systems Technology, University of Maryland, Baltimore County, NASA/GSFC TRMM Office, Greenbelt, Maryland.

Corresponding author address: Richard H. Johnson, Department of Atmospheric Science, Colorado State University, Fort Collins, CO 80523-1371.
E-mail: rhj@vortex.atmos.colostate.edu

Tropical cumulonimbus clouds are also often organized into larger-scale patterns such as squall lines or mesoscale convective systems (Zipser 1969, 1977; Houze 1977; Leary and Houze 1979).

The trade wind regimes have been studied for nearly three-quarters of a century, going back to the *Meteor* expedition of 1924–26 [see discussions by Riehl et al. (1951) and Malkus (1962)]. Using data from this early expedition, von Ficker (1936) demonstrated that water vapor is accumulated in the trades, but the primary release of latent heat through condensation of this vapor occurs within deep convection in the equatorial trough zone. The shallow cumulus clouds of the trade wind regime do condense water, but their primary role is to transport moisture upward toward the trade inversion layer to offset subsidence drying (Riehl et al. 1951; Augstein et al. 1973; Holland and Rasmussen 1973; Nitta and Esbensen 1974; Betts 1975). Water vapor from the trade wind layer then converges in the deep Tropics to become the fuel for "hot towers" (Riehl and Malkus 1958). Riehl and Simpson (1979) determined that 1600 to 2400 nearly undilute, giant cumulonimbus clouds are

HADLEY CIRCULATION
SHOWING ITCZ FIREBOX-CONDENSATION
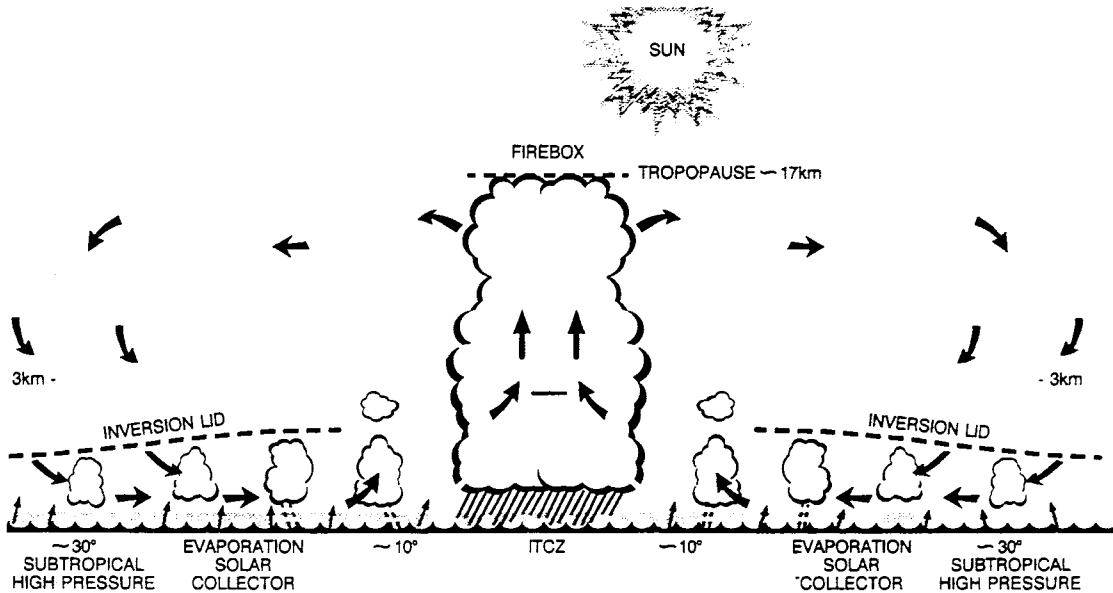## TRADE-WIND SOLAR COLLECTOR-EVAPORATION

FIG. 1. Schematic north–south slice through the tropical atmosphere showing the towering rainclouds in the ITCZ "firebox" (not to scale). Arrows show the meridional Hadley circulation, whose upper branch transports some of the released heat energy poleward in both hemispheres (Simpson 1992).

required daily to provide the essential vertical transport of total heat energy to satisfy the energy balance of the equatorial trough zone.

This view of the cooperative roles of the trade wind cumulus and equatorial cumulonimbus regimes is illustrated in Fig. 1 (from Simpson 1992). Depicted are trade cumuli capped by a trade inversion, convection in the Intertropical Convergence Zone (ITCZ), and the accompanying meridional circulation. Also shown in Fig. 1 is overshooting and dissipation of cumulus turrets above the inversion, a process demonstrated by Malkus (1954, 1958) to be important to the equatorward deepening of the trade cumulus layer.

The depiction in Fig. 1 is very useful for understanding the energetics of the tropical circulation. However, it was recognized early on (e.g., Malkus 1962; Malkus and Riehl 1964) that an abundance of other cloud types (midlevel or *cumulus congestus clouds*[1]) exist in the Tropics. These findings were later supported by the Global Atmospheric Research Program Atlantic Tropical Experiment (GATE) radar studies of tropical convection (e.g., Houze and Cheng 1977). Nevertheless, a number of conceptual models of tropical cloud populations have been proposed, within the context of the

Hadley circulation (e.g., Schubert 1976; Randall 1980; Emanuel 1994), that emphasize two primary cloud populations: shallow cumulus and cumulonimbus. *It is the purpose of this paper to draw renewed attention to cumulus congestus clouds in the Tropics and relate all three convective cloud types—cumulus, congestus, and cumulonimbus—to the thermal stratification of the tropical atmosphere.*

As indicated in Fig. 1, the trade inversion slopes gently upward toward the equator at 300–400 m (1000 km)$^{-1}$. These estimates of the inversion slope are based on observations taken from the eastern Pacific and western Atlantic trade wind zones (Riehl et al. 1951; Malkus 1958, 1962; Neiburger 1960; Firestone and Albrecht 1986; Schubert et al. 1995). Nearer the equator, data from the eastern Pacific from 0° to 15°N indicate that the height of the trade inversion is relatively constant (Kloesel and Albrecht 1989). Later, it will be seen that this finding also holds for the western Pacific. It has been argued by Kloesel and Albrecht (1989) and Sun and Lindzen (1993) that subsidence in regions surrounding deep convection in the ITCZ maintains the relatively low inversions in that region. This argument represents a purely thermodynamical view of the trade inversion, where the height of the inversion is controlled by a balance between large-scale subsidence tending to shallow the layer and moist convective and radiative processes tending to deepen it, the latter being a function of the cloud fraction (Malkus 1962; Betts 1973; Al-

---

[1] Cumulus congestus clouds are defined as cumulus clouds that are markedly sprouting and are often of great vertical extent; their bulging upper part frequently resembles a cauliflower (WMO 1956).

brecht et al. 1979; Schubert et al. 1979a; Sarachik 1985; Betts and Ridgway 1988; Bretherton 1993). This view assumes that the boundary layer depth and thermodynamic structure are controlled by *local* values of SST and large-scale divergence (Schubert et al. 1995). Within the subtropics, horizontal advection is also important since entrainment can occur not only by subsidence but also by horizontal flow across a sloping inversion (Neiburger et al. 1961; Riehl 1979; Schubert et al. 1979b; Wakefield and Schubert 1981; Albrecht 1984; Schubert et al. 1995).

An alternate, coupled dynamic–thermodynamic view of the quasi-horizontal structure of the trade inversion in the deep Tropics has been provided by Schubert et al. (1995). Because of its high static stability, the trade inversion in the subtropics represents a layer of high potential vorticity (PV). Schubert et al. argue that the trade inversion layer is strongly coupled horizontally since its stability is dynamically extended into the Tropics through the PV invertibility principle. In this view, rather than being controlled locally, the trade inversion height is controlled by *horizontally averaged* values of SST, divergence, and above-inversion atmospheric structure.

b. Marshall Islands and GATE results

Following these early studies of tropical cloud populations, a number of investigations of convection in the western Pacific were carried out using sounding data from the Marshall Islands region (Reed and Recker 1971; Nitta 1972; Yanai et al. 1973; Ogura and Cho 1973). In a diagnostic study of the bulk properties of cumulus ensembles in the tropical western Pacific, Yanai et al. (1973) found that in terms of cloud mass fluxes and detrainment, the population of cumulus clouds in the Tropics is predominantly bimodal; that is, shallow and deep cumulus clouds are the two dominant cloud types. Further study supported this idea (Yanai et al. 1976). Interestingly, however, the latter paper, upon examining the sensitivity of cloud diagnostic results to the assumed radiative heating profile, found a tertiary population of cumulus clouds detraining near 500 mb. Also, Johnson (1976), in applying a cloud diagnostic model to the western Pacific data of Reed and Recker (1971), found a maximum in the evaporation of detrained liquid water from cumulus updrafts in a layer between 400 and 600 mb. Thus, there is some evidence from these west Pacific studies of a third important detrainment level in the Tropics in the midtroposphere. Within the context of the cloud models used in these diagnostic studies, this midlevel detrainment can be interpreted as a population of congestus clouds. However, more generally, it may be thought of as a combination of detrainment from both congestus cloud tops and the sides of deeper clouds. This combined view is supported by cloud photographs taken during flights over the western tropical Pacific by Malkus and Riehl (1964) showing

numerous clouds topping out in the midtroposphere as well as frequent cloud shelves along the edges of cumulonimbus clouds (suggesting detrainment) between 400 and 500 mb.

GATE has provided additional statistics regarding tropical cloud populations. In particular, the size spectrum of radar echoes in the Tropics (whether measured in terms of echo areas, heights, durations, or rainfall intensities) has been found to be approximately lognormal (Lopez 1977, 1978; Houze and Cheng 1977; Warner and Austin 1978; Houze and Betts 1981). The lognormal distribution is characterized by a single peak at the small scales (many shallow cumulus) and progressively fewer numbers at the larger scales. It is hypothesized that this distribution can be explained as an aggregation of smaller clouds into larger ones (Lopez 1977). The frequency distribution of the maximum heights of radar echoes during GATE [Figs. 6 and 7 of Houze and Cheng (1977)] exhibits approximate lognormality, with the exception of a truncation at the deep-cloud end due to the tropopause (Lopez 1977). However, slight departures from lognormality also exist at the other end of the spectrum. Specifically, the distributions of maximum echo height for phases I, II, and III of GATE [Fig. 20 of Houze and Cheng (1977)] contain evidence of weak bimodality in the low to midtroposphere with peaks near 2–3 km and 5–7 km. The midlevel peak, consisting of cumulus congestus clouds, has been documented by Warner et al. (1980) to be a prominent cloud type within the cloud cluster on day 261 of GATE. The shallower peak represents only a small portion of the shallow cumulus population, most of which consists of nonprecipitating clouds. The abundant radar-echo tops in the 4–9-km range (60% of the total population for Houze and Cheng's entire GATE results) suggest that the traditional view of a simple bimodal distribution of tropical clouds needs revision, a concept that will be elaborated upon later with results from the recent Tropical Ocean Global Atmosphere Coupled Ocean–Atmosphere Response Experiment (TOGA COARE; Webster and Lukas 1992)

The GATE radar results are supported by sounding diagnostic studies. For example, Thompson et al. (1979, their Fig. 13) present the vertical distribution of horizontal divergence for a composite easterly wave. Three distinct layers of divergence are evident in the troposphere, which led them to infer that ''. . . [there are] three main populations of convective clouds in the GATE region with tops characteristically near 800, 500 and 250 mb.'' They also go on to say that ''This inference is supported by visual observations which revealed that convection gave rise to multiple cloud layers more often in the eastern Atlantic than in other tropical regions, but whether these layers tended to occur at three particular levels is not known.'' Abundant cloudiness in GATE was confirmed by Holle et al. (1979), who found using whole-sky camera data that on the average 79% of the sky was obscured by clouds during phase

III.[2] However, obscuration of higher clouds by lower clouds made it difficult to determine the precise area coverages of clouds at different levels.

A similar trimodal structure to the GATE divergence profile was reported by Nitta (1978, his Fig. 13) and Esbensen et al. (1982, their Fig. 3b). The latter study used the sounding dataset based on the statistical interpolation procedure of Ooyama (1987). Diagnoses of cumulus mass fluxes based on the Ooyama dataset indicate the relatively frequent occurrence of clouds that detrain in the midtroposphere, say, between 500 and 600 mb (e.g., Cheng 1989). Similar findings were obtained by Johnson (1980, his Fig. 14) using the Thompson et al. (1979) dataset. Shallow clouds were found to be abundant near the easterly wave ridge, whereas detrainment from both deep and midlevel cumulus clouds dominated in the wave trough. The levels of these three detrainment peaks approximately correspond to the levels of the divergence maxima found by Thompson et al. (1979). The relationship between detrainment level and cloud top is not necessarily one to one; nevertheless it is well known that for certain cloud types—shallow cumulus and cumulonimbus—substantial detrainment is concentrated near cloud top.

In summary, both the Marshall Islands and GATE studies provide evidence of abundant radar-echo tops and cloud detrainment in the midtroposphere. These findings suggest that cumulus congestus are at least as deserving of attention as shallow cumuli and cumulonimbi in conceptual models of tropical cloud populations. With this background, we now look to TOGA COARE data to see if additional light can be shed on this matter.

2. Mean statistics from TOGA COARE and comparison with GATE

One of the objectives of TOGA COARE was to determine the processes that organize convection over the western Pacific warm pool (Webster and Lukas 1992). Understanding the cloud populations themselves is an important first step in this task. Here we refer to ship-based radar and sounding data to describe and explain the nature of these cloud populations.

a. Radar data

Radar reflectivity data were collected from the Massachusetts Institute of Technology (MIT) C-band Doppler radar aboard the R/V *Vickers*. The radar operated for three ~30–day periods during the 4-month intensive observation period (IOP) (November 1992 through February 1993). Details regarding the data collection strat-

egies and data processing can be found in Rutledge et al. (1993) and Rickenbach and Rutledge (1998).

Before proceeding, it is important to understand what aspects of cloud populations the radar can and cannot measure. For both COARE and GATE, cloud properties are inferred from 5-cm radar data. However, since these radars detect only precipitation-sized particles, actual cloud top is only approximate. For convective clouds, cloud top and radar-echo top may often correlate well. For example, during the growing phase of a congestus cloud, cloud top and radar-echo top may be within 500 m of each other (Kingsmill and Wakimoto 1991). On the other hand, during the decaying phase of a cumulonimbus cloud, the two tops may differ significantly. Likewise, for other cloud types (e.g., nimbostratus, cirrus) the correlation between radar-echo top and cloud top can be poor. Therefore, statistics involving radar-echo tops may be quite different than those for cloud tops, especially considering the full range of cloud types (convective and nonconvective) that exist in the Tropics. Ultimately, meaurements from precipitation radars, cloud radars, satellites, and other sensors will have to be integrated to obtain a more complete description of tropical cloud systems. Nevertheless, the radar-echo top data presented in this study are felt to provide a valuable general description of the distribution of tropical *convective* clouds over the warm pool during COARE.

In order to determine the characteristics of COARE cloud systems, Rickenbach and Rutledge (1998, hereafter RR98) applied the objective technique of Steiner et al. (1995) to separate "convective" from "stratiform" precipitation features within rain systems. With this technique, horizontal maps of radar reflectivity are examined for regions of high reflectivity or strong reflectivity gradients, criteria that are used to determine the location of convective cells. Contiguous points determined to be convective cells are defined as a *convective feature*. Convective features are composed of individual cells or small groups of cells. An analysis of the size distribution of convective features (not shown) indicates that the majority defined by the objective separation technique are of relatively small horizontal scale: 95% (80%) are less than 25 (15) km in length, respectively. Hence, many of the convective features are made up of just one or a few cells. There were extended periods during the COARE IOP when only isolated cells existed over the intensive flux array (IFA) (e.g., undisturbed, light-wind periods). Since the objective separation technique tends to classify many of the weaker cells at these times as stratiform, RR98 assign all echoes during the isolated-cell periods as convective.

A plot of the frequency distribution of convective feature echo heights based on MIT radar data for all of COARE is shown in Fig. 2.[3] The COARE data are based

---

[2] McGuffie and Henderson-Sellers (1989) note that this value is an overestimate due to complications in cloud cover computations near the horizon.

[3] Figure 2 contains reflectivity volume scan data at 20-min intervals for 80 days, or nearly 6000 volumes.
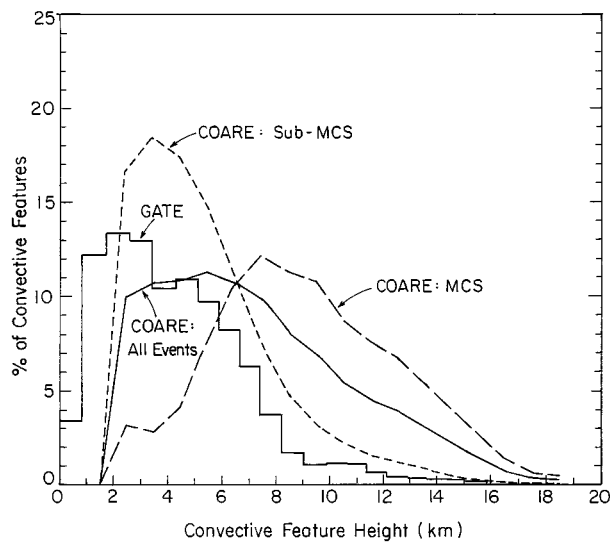
FIG. 2. Frequency distribution of maximum heights of radar echoes for all three phases of GATE (Houze and Cheng 1977) and instantaneous radar-echo heights for all three cruises of the R/V *Vickers* during COARE (Rickenbach and Rutledge 1997a). COARE results are also subdivided into sub-MCS and MCS categories, which represent contiguous convective echo patterns less than or greater than 100 km in horizontal dimension, respectively.

on instantaneous snapshots of the reflectivity field at 20-min intervals. A similar procedure was used in a study of radar echoes in the Barbados area by Lopez (1976). Also, DeMott and Rutledge (1998a) prepared similar plots of echo-height distributions for all three cruises of the *Vickers*. For convective features containing more than one cell, the height of the tallest echo is recorded. Since convective features with multiple cells typically involve deep-cloud systems, there are actually more cells than features at the tall-echo end of the COARE spectrum in Fig. 2. This point will be important in interpreting the deep-cloud or cumulonimbus portion of the tropical cloud distribution later.

Curves for COARE in Fig. 2 are given for all cases (*all events*) as well as two classifications of echo type, sub-MCS and MCS. The sub-MCS category refers to features whose adjacent convective precipitation echoes are <100 km in horizontal scale, whereas MCS features contain adjacent convective echoes ≥100 km in scale [following the definition of Houze (1993)]. RR98 note that while the sub-MCS classification is the most common (occurring 56% of the time), the MCS category contributes by far the most rainfall (84%). The COARE all events curve shows a broad maximum between 2 and 8 km, with a weak peak at 5.5 km. DeMott and Rutledge (1998a) show that this distribution is similar for all three cruises of the *Vickers*, but the peak is slightly lower (4–5 km) for cruise 1, when conditions were less disturbed, than the last two cruises, which had peaks near 7–8 km. The sub-MCS and MCS subdivisions show that the broad maximum consists of two populations: a shallow echo type (sub-MCS) with a peak at 3.5 km

and a deeper echo type (MCS) with a peak at 7.5 km (MCS also exhibits a secondary peak at 2.5 km). These results indicate that, on average, isolated (sub-MCS) convective features are shallower than those organized on the MCS scale. The shallow clouds are most prevalent during the inactive or suppressed phase of the 30–60-day intraseasonal oscillation (ISO) when the large-scale vertical motion is weak or downward (Figs. 9 and 11, later).

Also shown in Fig. 2 is the frequency distribution of *maximum echo height* derived from reflectivity data from the C-band radar aboard the R/V *Oceanographer* during GATE (Houze and Cheng 1977).[4] The most common radar-echo top in GATE is between 2 and 3 km with a weak secondary maximum near 5 km. Also, the GATE echo heights are shifted to somewhat lower values than those in COARE. Since instantaneous heights often differ from maximum heights attained by echoes, some of the differences in the GATE and COARE frequency distributions can be attributed to differences in processing procedures. For example, all else being the same, a frequency distribution of maximum echo height (GATE) should be skewed to higher values than a distribution of instantaneous heights (COARE) for the same population. But this is just the opposite of what is observed in Fig. 2. Therefore, another explanation is needed, which will be dealt with momentarily. On the other hand, the greater sensitivity of the MIT radar might be expected to lead to a taller echo population in COARE than GATE. Also, while the GATE and COARE data were both obtained with C-band (5 cm) radars, there are differences in the radar characteristics (minimum detectable signal, beamwidth, etc.) as well as the time of observations (COARE data are for all times of day; GATE echoes are tracked from 1200 UTC). It is hard to judge the impact of all of these factors on the frequency distributions.

However, returning to the skewing of the COARE distribution to higher echo heights, there may be a simple explanation not related to the radar characteristics or analysis techniques. Specifically, the existence of a greater percentage of deeper echo tops in COARE than GATE is consistent with the ~3 K higher SST and ~2 km higher tropopause over the western Pacific warm pool than in GATE.[5] The deeper clouds in COARE than GATE are also reflected in a higher level of the peak in the mean apparent heat source Q_1 for COARE (near 6 km) as opposed to 4 km for GATE (Lin and Johnson 1996b).

---

[4] Houze and Cheng (1977) tagged each echo present at 1200 UTC and tracked it back and forth in time to the maximum height attained in its lifetime.

[5] Higher SSTs do not automatically imply deeper clouds. For example, water loading, vertical wind shear, etc., can affect the ultimate heights of clouds. However, the higher tropopause in COARE is one indication that clouds there grow to higher levels.
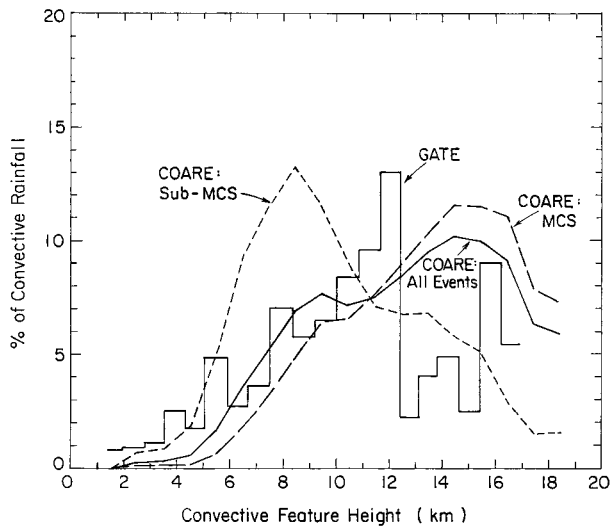
FIG. 3. As in Fig. 2 except for percent contribution to total convective rainfall.

Despite these differences between GATE and COARE frequency distributions, there is one important commonality: both show significant populations of echo tops in the midtroposphere. For both GATE and the subdivided COARE distributions, there are peaks at the shallow end (between 2 and 3.5 km) and in the midtroposphere (between 5 and 7.5 km). However, irrespective of the actual locations of these peaks, we conclude that *the overall midlevel echo maximum, representing cumulus congestus clouds, constitutes a significant fraction of the tropical cloud population. Specifically, congestus clouds with tops between 4.5 and 9.5 km represent 57% of the precipitating convective clouds in COARE.* Despite the difference in analysis techniques, these results compare favorably with those of Houze and Cheng (1977), where 60% of GATE radar-echo tops fell between 4 and 9 km. For the GATE results (Houze and Cheng 1977), there is actually a very minor third peak near 11 km. A similar third peak cannot be seen in the COARE data, but since those results are for convective features and, as mentioned earlier, there can be more than one echo in some of the tall features, deep echoes are somewhat undercounted in the COARE distributions. Whether the third peak exists prominently or not in the frequency distributions, deep convection is well known as a ubiquitous feature of the Tropics.

While tall echoes appear to be insignificant in terms of their numbers in Fig. 2, *they are not insignificant* when viewed in terms of percent contribution to total convective rainfall (Cheng and Houze 1979). This result is shown in Fig. 3. Both GATE (Cheng and Houze 1979) and COARE (RR98) show very prominent convective rainfall peaks for echoes with tops between 12 and 16 km (near the tropopause). Cheng and Houze (1979) attribute the two peaks at 12 and 16 km in GATE to clouds that do not and do, respectively, overshoot the tropo-

pause. These deep echoes are few in number, but they contribute significantly to the total rainfall (Houze and Cheng 1977; Lopez 1978; Houze and Betts 1981; RR98; DeMott and Rutledge 1998b). There is also a large contribution to total convective rainfall by echoes with tops between 8 and 12 km. These peaks correspond to the large population of midlevel clouds, the taller of which produce proportionately more rainfall. However, it is important to note that *for the entire population of COARE clouds as sampled by the ship radar, cumulus congestus clouds (defined here as echoes with tops between 4.5 and 9.5 km) contribute over one-quarter (28%) of the total convective rainfall over the warm pool.* A similar result (30%) is obtained for echo tops between 4 and 9 km in GATE (Cheng and Houze 1979). For the sub-MCS category, many of which represent isolated cells, the fraction is even greater, 52%, or over half the total convective rainfall of that category. In other words, many of the isolated cells in COARE are of the congestus cloud variety that often produce heavy rain, presumably due in part to the effective warm-rain processes over the exceptionally warm ocean in this part of the world. Of course, the deepest of these clouds glaciate so that ice processes are also important in their rainfall production.

To summarize, analyses of GATE and COARE radar-echo tops reveal a substantial contribution by cumulus congestus clouds to the total cloud population. However, considering that the C-band radars do not detect nonprecipitating clouds, it is not clear how populous the congestus are in relation to shallow cumulus. They are certainly more abundant than cumulonimbus (Fig. 2), even though the latter contribute a greater fraction of the total rainfall (Fig. 3). But just how do they compare to the large numbers of shallow, nonprecipitating cumuli? In order to establish a crude comparison, the nonprecipitating component is estimated based on two assumptions of shallow cumulus densities for the COARE region, 1 and 10 clouds $(10^2 \ km^2)^{-1}$ These estimates are intended to roughly represent shallow cumulus densities based on GATE ''fair-weather'' conditions (Nicholls and LeMone 1980), where an average cumulus diameter of 1 km is assumed. Williams et al. (1996) report that the shallow, nonprecipitating clouds during relatively undisturbed conditions in COARE were similar to the GATE fair-weather cloud fields. Of course, the shallow cumulus field is modified by disturbances such that the IOP-mean population is difficult to determine accurately. A plot of these two estimates of shallow cumulus populations is shown in in Fig. 4 along with the COARE all events curve for radar-echo tops. Two peaks can be seen, corresponding to shallow cumulus and cumulus congestus clouds. Had the subdivided sub-MCS and MCS populations been plotted in Fig. 4 instead, the two peaks would even be more distinct since the sub-MCS maximum near 3.5 km (Fig. 2) would blend in with the shallow cumulus peak and the MCS maximum near 7.5 km would be more isolated. Since
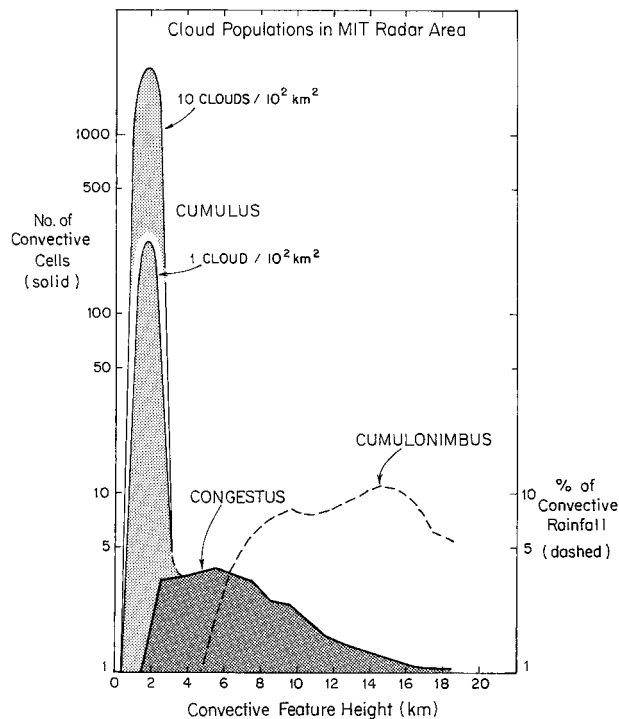
FIG. 4. Average number of clouds in the MIT radar area (solid curves) and percent of convective rainfall (dashed curve) as a function of convective feature height. The frequency distribution of precipitating convective features, containing a congestus peak (marked CONGESTUS), is from Fig. 2. The percent contribution to convective rainfall, with a peak at the cumulonimbus end (marked CUMULONIMBUS) is from Fig. 3. Two cumulus distributions (marked CUMULUS), based on shallow cloud densities of 1 and 10 $(10^2 \text{ km}^2)^{-1}$, are estimated from information and data in Williams et al. (1996) and Nicholls and LeMone (1980).

deep echoes are few in number, they do not show up as a peak in the number frequency in Fig. 4. But since deep echoes are undercounted due to multiple echoes in tall convective features, a complete count may actually show a third peak in the upper troposphere if Fig. 4 were a plot of the frequency distribution of *echo* instead of feature heights. Regardless, cumulonimbus are important to the total rainfall, and to emphasize this, we depict them in Fig. 4 by plotting the COARE all events curve for percent convective rainfall (Fig. 3). Figure 4 is meant to illustrate that cumuli, congestus clouds, and cumulonimbi are all important components of the tropical cloud spectrum, the first two for their abundance and the last for the rainfall they produce. We next examine in some detail how these cloud populations relate to the thermal stratification of the tropical atmosphere.

b. Sounding data and related analyses

Plots of the static stability over the TOGA COARE IFA during the IOP and for the GATE easterly wave composite of Thompson et al. (1979) are shown in Figs. 5a and 5b (computed using 25-mb data in both cases).

The COARE results (Fig. 5a) indicate three levels of enhanced stability, corresponding to the trade wind inversion (2 km), the 0°C level (~5 km), and the tropopause (~16 km). The weakest of the three, near the 0°C level, is related to the effects of melting (Johnson et al. 1996). The GATE composite easterly wave data also exhibit a three-layer structure (Fig. 5b), although the upper two peaks are at slightly lower levels, corresponding to the fact that the 0°C level is about 0.5 km lower and the tropopause ~2 km lower in GATE (presumably due to the lower SSTs in the eastern Atlantic).[6] Also, note that the trade stable layer in the GATE composite is strongest in the easterly wave ridge region, consistent with the maxima in low-level divergence and cumulus detrainment in that position (Thompson et al. 1979; Johnson 1980). These three stable layers generally correspond to the two peaks in the frequency distribution of radar-echo tops (Fig. 4) and the cumulonimbus population. Specifically, the GATE peak near 2 km and the COARE sub-MCS peak near 3.5 km in Fig. 2 correspond to the trade wind stable layer, allowing for some overshooting. The tropopause, of course, marks the upper limit of cumulonimbus growth. The weakest of the three stable layers (near the melting level) has a broad echo-top peak associated with it (the COARE all events curve in Fig. 2), but a somewhat sharper peak ~2.5 km above it in the COARE MCS curve.

The correspondence between the three stable layers and radar-echo tops suggests a cause and effect relationship. In particular, it is proposed that the stable layers are of sufficient strength to retard or limit cloud growth, especially under conditions of weak low-level forcing (e.g., Johnson et al. 1996; Zuidema 1998). It is well known that the trade wind *inversion* (where the temperature actually increases with height) and tropopause severely inhibit cloud growth, leading to detrainment near those levels (Malkus 1958; Malkus and Riehl 1964). However, the trade stable layers in COARE and GATE (Fig. 5) do not typically exist as true temperature inversions. Nevertheless, they do have large populations of tradelike, precipitating cumuli associated with them, as indicated in Fig. 2, and abundant nonprecipitating shallow cumuli as illustrated in Fig. 4. In a study of clouds during day 261 of GATE, Warner et al. (1980) noted that stable layers at 2.2 and 5 km acted as "barriers" to penetration by cumuli, with considerable stratiform debris observed near the 5-km level.

Let us briefly consider the shallow cumulus population in more detail. Further analysis of this cloud population by Johnson and Lin (1997) indicates the existence of two types of shallow cumulus during the COARE IOP. One type occurs during high-wind periods or westerly wind bursts. At those times, substantial "ap-

---

[6] The fields in Fig. 5b are smoother than those in Fig. 5a because only eight wave categories are analyzed in the former as opposed to 480 observation times in the latter.
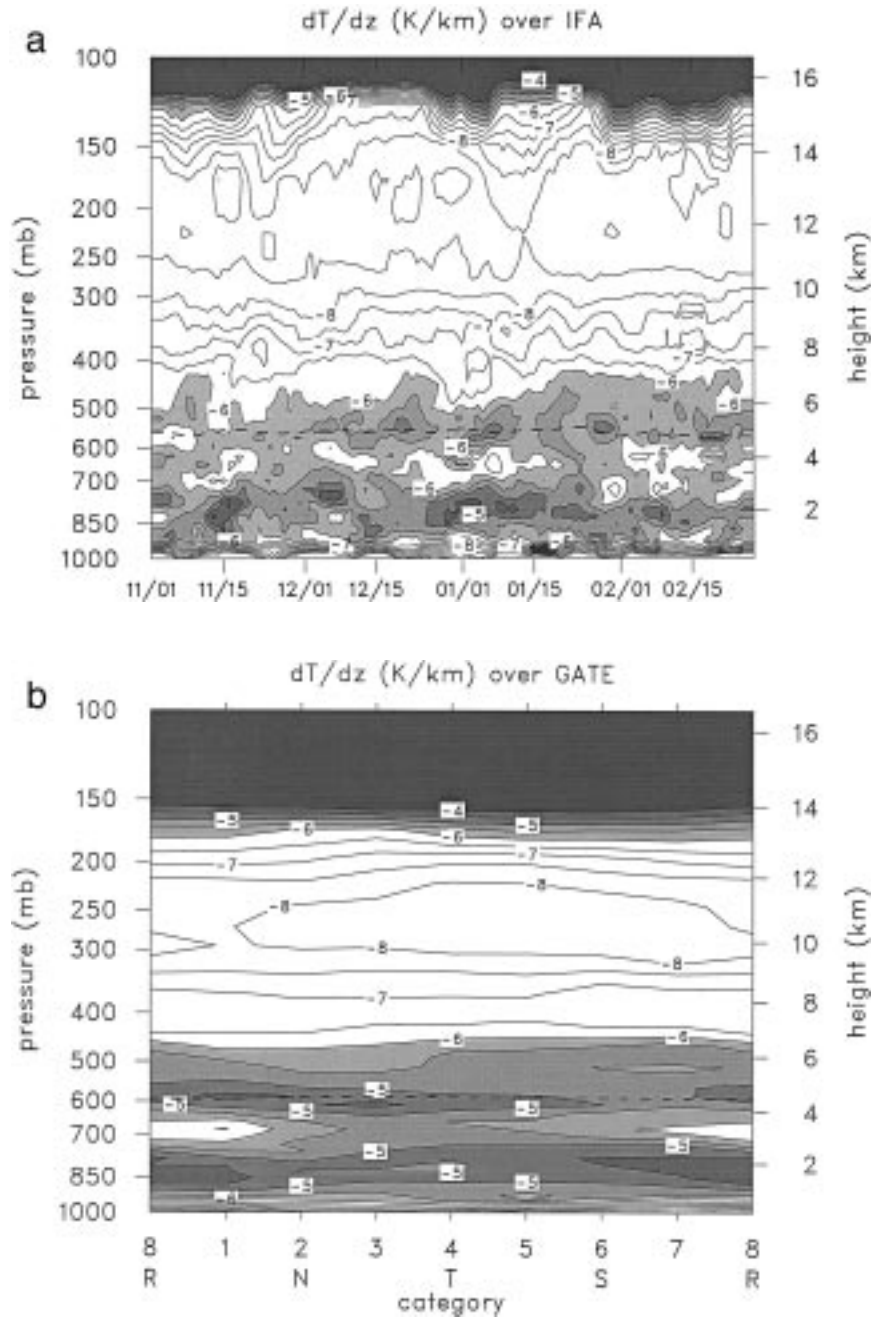
FIG. 5. (a) Time series from 1 Nov 1992 to 28 Feb 1993 of *dT/dz* computed by averaging 25-mb gridded data (1° horizontal resolution) over the COARE intensive flux array. Darker shading indicates regions of greater stability with a contour interval of 0.5 K km⁻¹. Dashed line indicates 0°C level (Johnson et al. 1996). (b) As in (a) except for eight categories of Thompson et al. (1979) composite easterly wave (4 = wave trough, 8 = wave ridge).

parent moistening'' [negative Q_2, following Yanai et al. (1973)] is found near cloud base in association with ''subinversion'' (Esbensen 1978) or ''forced'' (Stull 1985) type cumuli that are largely a manifestation of overshooting, mechanically driven, boundary layer ed-dies. In contrast, during suppressed, light-wind periods, slightly deeper cumuli [''inversion penetrating'' after Esbensen (1978) or ''active'' after Stull (1985)] are found with apparent moistening peaking in the upper part of the cloud layer (similar to the Atlantic trades;

Nitta and Esbensen 1974). Latent heating plays an important role in the evolution of the active trade cumulus clouds. Higher SST (by 1 K) and weaker wind shear during the latter periods likely contributed to the more active cumulus at that time. These two populations of trade cumulus, forced and active, have been depicted in a conceptual model of the trade-to-ITCZ cloud transition by Randall (1980).

The stable layers near the 0°C level are the weakest of the three in Fig. 5 for both COARE and GATE. Seemingly, therefore, they might not be expected to significantly impact cloud development. However, there is evidence to indicate otherwise. In particular, it has been demonstrated that deep convection penetrating even relatively weak stable layers can lead to enhanced detrainment and moistening near those levels (Bretherton and Smolarkiewicz 1989; Taylor and Baker 1991; Raymond et al. 1991; Raymond and Blyth 1992). The peak in "cloudy layers" near the 0°C level inferred from COARE relative humidity data by Mapes and Zuidema (1996) supports this idea. Similar midlevel cloud layers or cloud shelves have been observed on trans-Pacific aircraft flights by Malkus and Riehl (1964), in the eastern Atlantic (Thompson et al. 1979), and in recent space shuttle lidar measurements over the western Pacific (Platt et al. 1999). The relatively weak melting-layer inversions can limit cloud growth because warm-pool cumulus congestus clouds are often strongly entraining and heavily loaded with precipitation, so that their buoyancy is often weak (Betts 1982; Xu and Emanuel 1989). Entrainment is effective in restricting cloud growth over the warm pool because of frequent midlevel dryness due to dry intrusions from the subtropics (Parsons et al. 1994; Numaguti et al. 1995; Yoneyama and Fujitani 1995; Mapes and Zuidema 1996).

Recently, Zuidema (1998) has used the buoyancy-sorting model of Raymond and Blyth (1992) to investigate cumulus detrainment profiles in the COARE region. Neglecting the effects of freezing, she finds a trimodal structure to the detrainment for COARE clouds (Fig. 6). This figure contains curves for three assumptions of maximum parcel hydrometeor mixing ratios: 1, 3, and 5 g kg^{-1}. As the maximum condensate carried within the parcel is increased, the parcel buoyancy decreases, leading to decreased detrainment at pressures below 750 mb and increased detrainment at pressures greater than 750 mb. The calculation with 1-g kg^{-1} hydrometeor mixing ratio, which is representative of condensate loading for shallow clouds, has a detrainment peak near 800 mb reflecting the effects of the trade stable layer. A midlevel detrainment peak is diagnosed near 400 mb ($\sim$7.5 km), very close to the peak in the MCS radar-echo top distribution (Fig. 2). While there is not a one-to-one correspondence between detrainment and echo top, the peak in the MCS curve in Fig. 2 near 7.5 km suggests that processes contributing to enhanced detrainment near that level (Fig. 6) may also contribute to restricting cloud growth
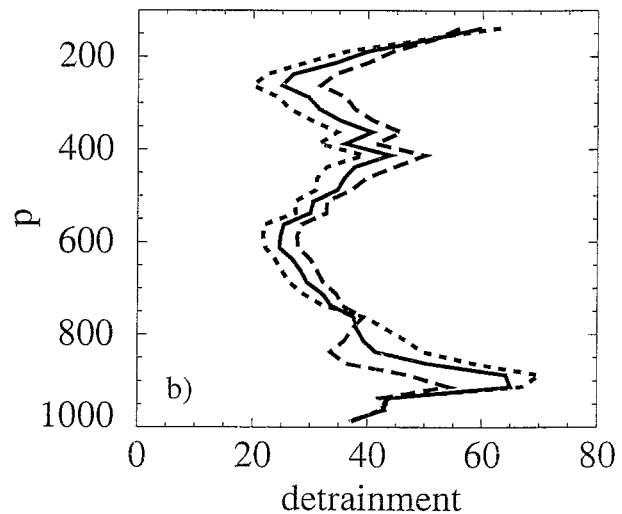

FIG. 6. Frequency distribution of the outflow levels of the total ensemble of diluted parcels for 485 soundings from Kapingamarangi, assuming liquid water condensation only. Dotted, solid, and dashed lines denote liquid water parcel maxima of 5, 3, and 1 g kg^{-1}, respectively (Zuidema 1998).

to that level, particularly for strongly entraining and heavily precipitation-laden congestus clouds that are common over the warm pool. Zuidema (1998) shows that if freezing is included when the temperature falls below 0°C, the midlevel peak vanishes, owing to the buoyancy-enhancing effects of the latent heat of fusion. However, many of the warm-pool congestus clouds may not glaciate until they reach temperatures of $\sim$ -15°C (the approximate 400-mb temperature), such that detrainment near and below this level is common. This argument is consistent with recent numerical modeling studies for COARE clouds, which indicate substantial concentrations of supercooled rain at temperatures as low as -10° to -15°C (W. Petersen 1997, personal communication). Therefore, the detrainment distribution in Fig. 6 may well be relevant to populations of nonglaciating congestus clouds in COARE. Typical photographs of the precipitating cumulus and cumulus congestus populations are shown in Fig. 7 (cumulus in Fig. 7a and congestus in Figs. 7b–d). Cumulus congestus clouds that do eventually glaciate get an additional boost of buoyancy and rise to higher altitudes, perhaps even the tropopause.

3. Temporal variability of radar-echo populations

A time series of divergence over the IFA reveals evidence of the three prominent radar-echo populations (Fig. 8). Most prominent is the divergence peak near 200 mb associated with deep cumulonimbus. Upper-level divergence is strongest during December, when there is pronounced low-level convergence accompanying the onset of an intense westerly wind burst (Gutz-

FIG. 7. Photographs taken from R/V *Vickers* of (a) cumulus with detrainment near cloud top on 29 or 30 Nov 1992 (by Charlotte DeMott); (b) and (c) cumulus congestus on 6–8 Feb 1993 (by Robert Cifelli); and (d) cumulus congestus on 28 Nov 1992 (by Charlotte DeMott).

ler et al. 1994; Lin and Johnson 1996a). Divergence peaks in the low to midtroposphere, presumably representing detrainment from cumulus and cumulus congestus clouds, are weaker and more sporadic, but they do exist.

In order to more closely examine the divergence maxima and their relationship to radar-echo tops, time series of the number of shallow, medium, and deep radar echoes have been prepared for the three cruises of the R/V *Vickers* and compared to fields of sounding-derived var-

iables. To illustrate these relationships, we present results for cruises 1 and 2 (10 November–10 December and 20 December–19 January). Results for cruise 3 (not shown) reveal similar relationships. Time series of the number of clouds within a 120-km radius of the MIT radar in three echo-top categories (low or cumulus, 0–4 km; middle or congestus, 5–9 km; high or cumulonimbus, 11–16 km) are shown in Fig. 9 along with a time series of the SST at the Improved Meteorological surface mooring (IMET) (Weller and Anderson 1996). Pe-
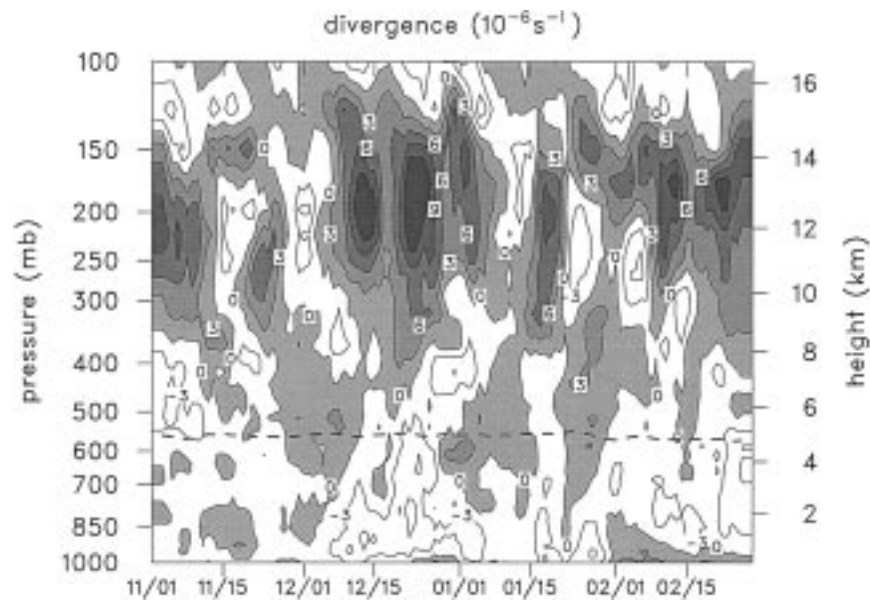
FIG. 8. Four-month time series of horizontal divergence over COARE IFA (5-day running means). Units are 10^{-6} s^{-1}; positive values are shaded.

riods when MCS-scale organization is present are denoted by solid segments in Fig. 9 (although some sub-MCS elements may also occur at these times), whereas periods of *only* sub-MCS echoes are denoted by dotted segments. Except for periods of disturbed weather on 22–25 November and 5–10 December (note increased numbers of deep clouds at those times), there is a general increasing trend in the number of cumulus and congestus clouds throughout the period, many of which are in the form of isolated cells. This period is generally characterized by light IFA-averaged rainfall, mostly clear skies, and increasing SST [Lin and Johnson (1996b) and bottom panel of Fig. 9]. Apart from the disturbed periods, there is a large (~1°–3°C) diurnal range in SST during cruise 1 as a result of very light winds and mostly clear skies (Weller and Anderson 1996; Soloviev and Lukas 1997). Shallow, precipitating clouds are most abundant when the diurnal cycle is large, and many of these clouds occur during the afternoon near the time of maximum SST (Rickenbach and Rutledge 1997; Sui et al. 1997).

The time series of vertical motion for the corresponding period (Fig. 10a) shows that mid- to lower-tropospheric subsidence prevails, except for the disturbed periods. Thus, the shallow cumulus and cumulus congestus clouds grow into a subsiding environment, much like trade cumulus regimes. As the cumulus and congestus populations increased toward the end of the period (Fig. 9), the divergence maximum near and just above the 0°C level strengthened (Fig. 10b), suggesting increased detrainment from these echo tops. Correspondingly, the moisture in the lower troposphere increased and the moist layer deepened, as indicated by the time series of

relative humidity (Fig. 10c).[7] This moistening evidently served to precondition the atmosphere for deep convection prior to the December westerly wind burst [Johnson and Lin 1997 (see time series of apparent moisture sink Q_2 in their Fig. 5); Godfrey et al. 1998; Lau and Sui 1997]. The trade stable layer is seen to rise throughout the period (Fig. 10d) as the populations of shallow cumulus increased (Fig. 9).

The evolution of the three radar-echo types and SST during cruise 2 is shown in Fig. 11. The period begins with low SSTs as a result of the late-December westerly wind burst, with a corresponding decrease in cumulonimbi, whose numbers reach zero by the end of the month. The reduction in deep echoes is consistent with low to midtroposphere drying during that period (Fig. 12c). However, the drying appears to be at odds with concurrent mean upward motion (Fig. 12a). This apparent inconsistency is explained by the occurrence of frequent dry intrusions from the subtropics during this time (Fig. 10 of Mapes and Zuidema 1996). Shallow, precipitating clouds virtually disappear at the end of December when the SST is near its minimum, coincident with the westerly wind burst (Lin and Johnson 1996a). However, nonprecipitating shallow cumulus are abundant at this time (Johnson and Lin 1997). During the first half of January there is an increase in the number of cumulus and congestus clouds as the SST

---

[7] Values of relative humidity (RH) at low levels may have a low bias of ~5% or more due to problems with the rawinsonde humidity sensors. However, this bias should not affect interpretations of the temporal behavior of RH shown in Figs. 10c and 12c.
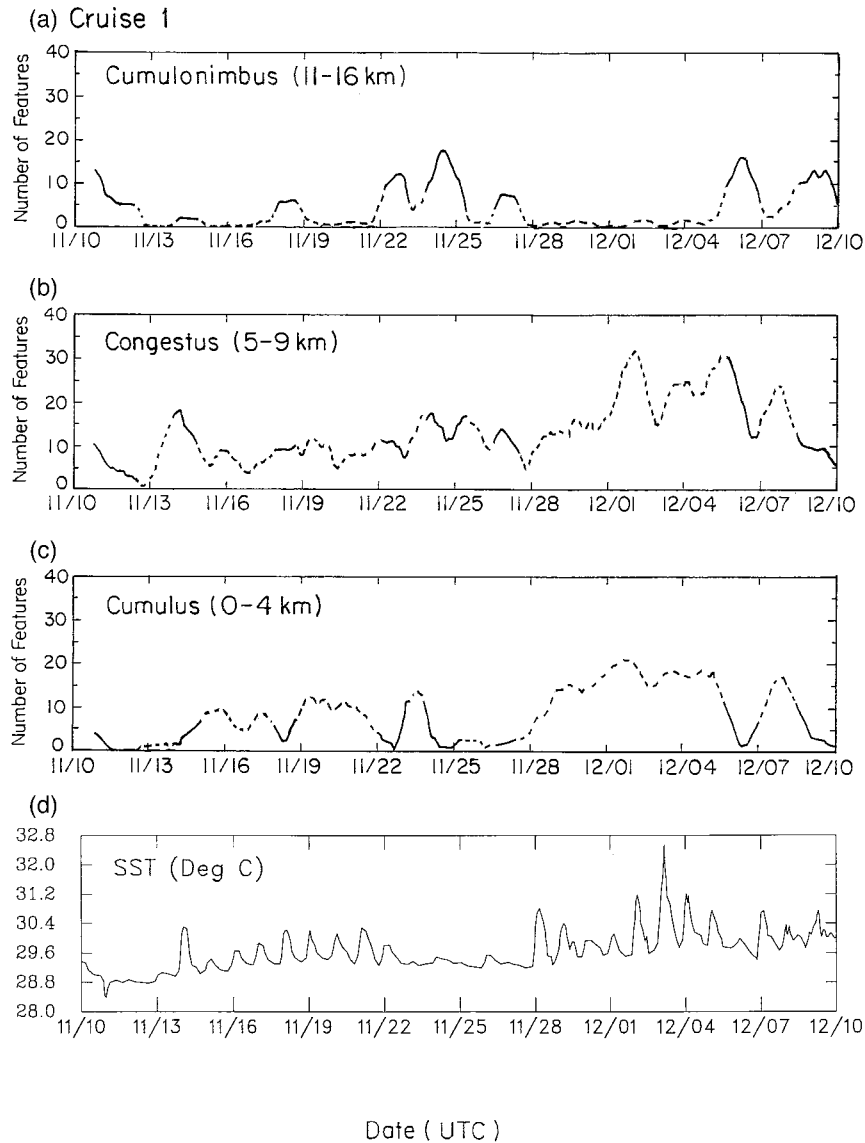
FIG. 9. Daily-averaged number of low or cumulus (0–4 km), middle or congestus (5–9 km), and high or cumulonimbus (11–16 km) radar-echo tops for cruise 1 of the R/V *Vickers,* and SST at IMET buoy at 2°S, 156°E. In upper three panels, solid curve segments refer to periods when convective echoes organized on the MCS scale (>100 km) and dotted segments to periods when only sub-MCS or isolated cells existed.

increases (Fig. 11), with an associated general moistening of the lowest 3 km of the troposphere (Fig. 12c). Congestus clouds are most prevalent when there is MCS organization and cumulonimbus activity (Fig. 11). This result is consistent with a corresponding strengthening of the 0°C stable layer at these times (Fig. 12d) from enhanced melting (Johnson et al. 1996). It also helps to explain why the MCS curve in Fig. 2 displays such a prominent peak near 7.5 km. In effect, the MCS-scale events self-modify their cloud-height distribution by producing melting-related stable layers that enhance the congestus population. However,

Figs. 9 and 11 indicate that congestus clouds exist even when the stable layer is weak (Figs. 10 and 12), suggesting that such clouds can exist independent of the 0°C stable layer, presumably due to the effects of water loading and entrainment. In this regard, the 0°C stable layer is viewed as *enhancing* the congestus population.

As in cruise 1, most of the cruise 2 clouds during the period of large diurnal SST variation (indicative of clear skies and light winds) are of the sub-MCS or isolated cell type, with a peak in echo tops near 3.5 km (Fig. 2). The height of maximum divergence in-
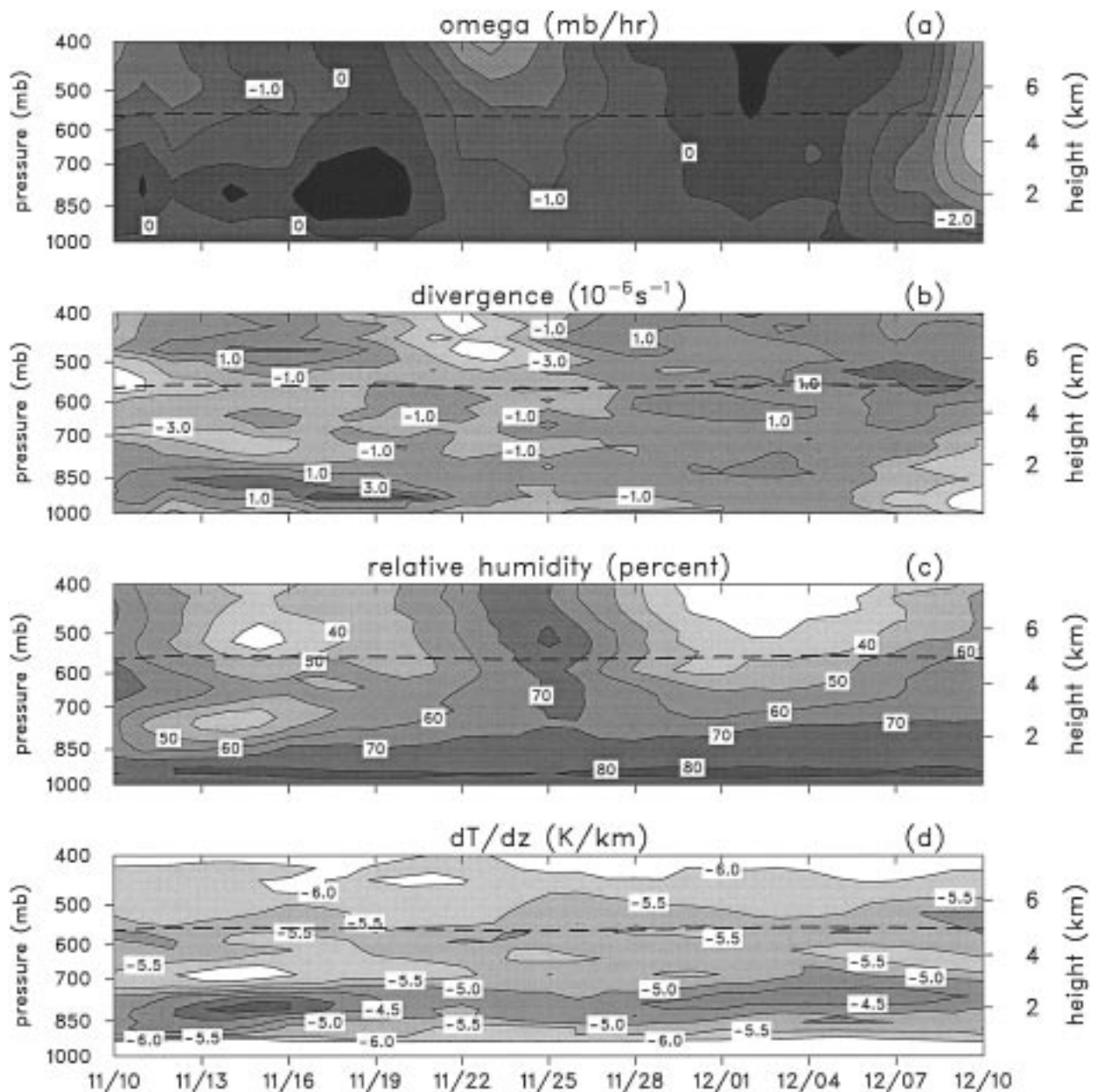
FIG. 10. Time series for cruise 1 of the R/V *Vickers* of (a) ω (mb h^{-1}), (b) horizontal divergence (10^{-6} s^{-1}), (c) relative humidity (%), and *dT/dz* (K km^{-1}). These fields (5-day running means) were computed from 1° resolution gridded sounding data averaged over the area covered by the MIT radar. Dashed line near 5 km indicates 0°C level.

creases through this period (Fig. 12b), suggesting a deepening cloud field. Also, the height of the trade stable layer increases (Fig. 12d) as the SST and number of cumuli increase during the first half of January. Finally, at the end of the period the number of tall echoes increases, accompanied by deepening lower-tropospheric convergence, upward motion, and moisture (Figs. 12a–c).

In summary, time series of radar and sounding data

for the time periods of cruises 1 and 2 of the R/V *Vickers* yield the following results.

• Cumulus cloud populations are modulated on the ISO and shorter timescales; shallow and deep cumulus vary the most.
• Precipitating shallow cumuli are suppressed during the westerly wind burst, then increase as the SST increases; the trade stable layer rises as the SST increases.
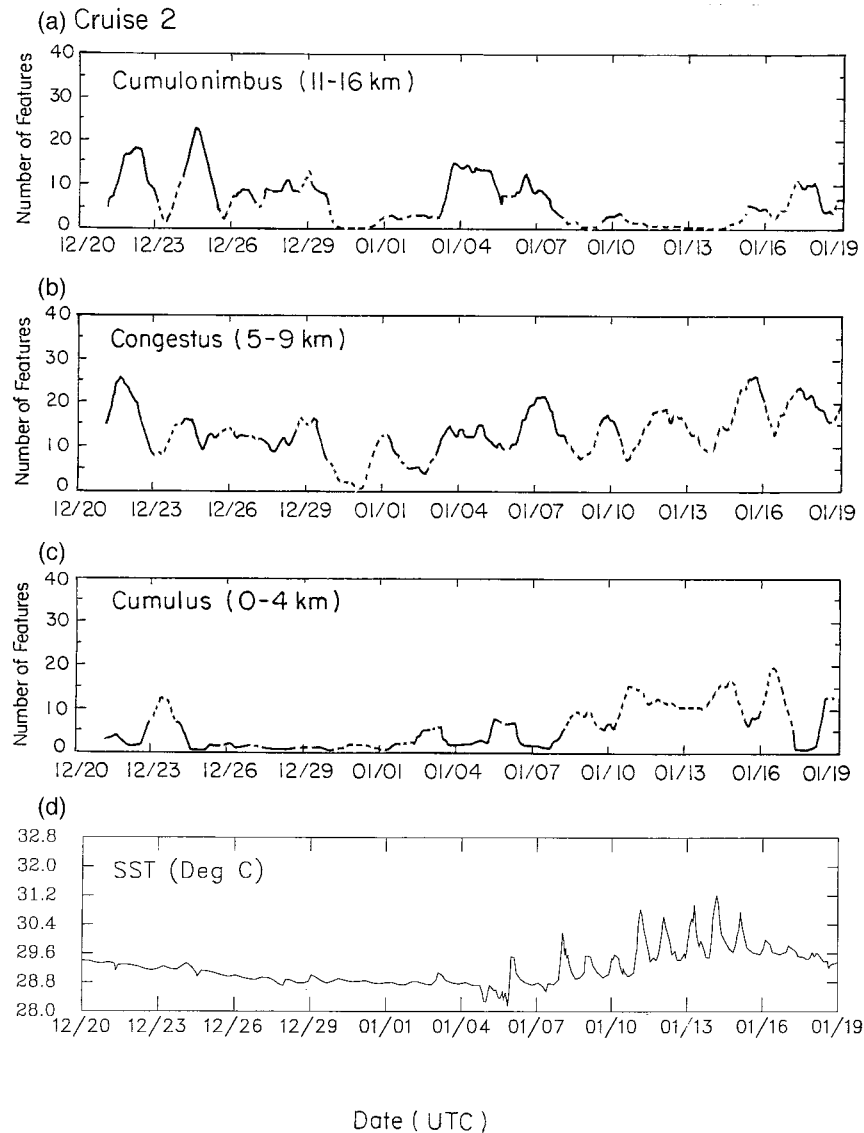
FIG. 11. As in Fig. 9 except for cruise 2 of R/V *Vickers.*

- Congestus clouds are prevalent at all times, increase as the SST increases, and along with shallow cumulus, moisten the lower troposphere, thus preconditioning it for deep convection. The congestus population peaks at times of MCS organization and when the 0°C stable layer is strongest.
- The diurnal cycle of SST is large when shallow cumuli are abundant (shallow cumuli peak in the afternoon; Rickenbach and Rutledge 1997; Sui et al. 1997); deep convection suppresses the diurnal cycle of SST.

4. Other corroborating results

The existence of a trimodal population of tropical clouds is supported by recent aircraft observations, lidar measurements, wind profiler analyses, and cloud-resolving modeling results. The National Aeronautics and Space Administration (NASA) DC-8 aircraft was used in 1991 to measure vertical distributions of water vapor, ozone, and other trace constituents over the tropical North Pacific Ocean (Newell et al. 1996). They detected a peak in the number of layers of water vapor–rich, ozone-poor air (indicative of convective transport from the boundary layer) between 4 and 6 km. These observations suggest enhanced detrainment in the midtroposphere, which may correspond to the cumulus congestus detrainment discussed earlier.

The lidar studies are still in progress, so detailed results are not yet available. The first relevant observations were taken during COARE from the Cloud
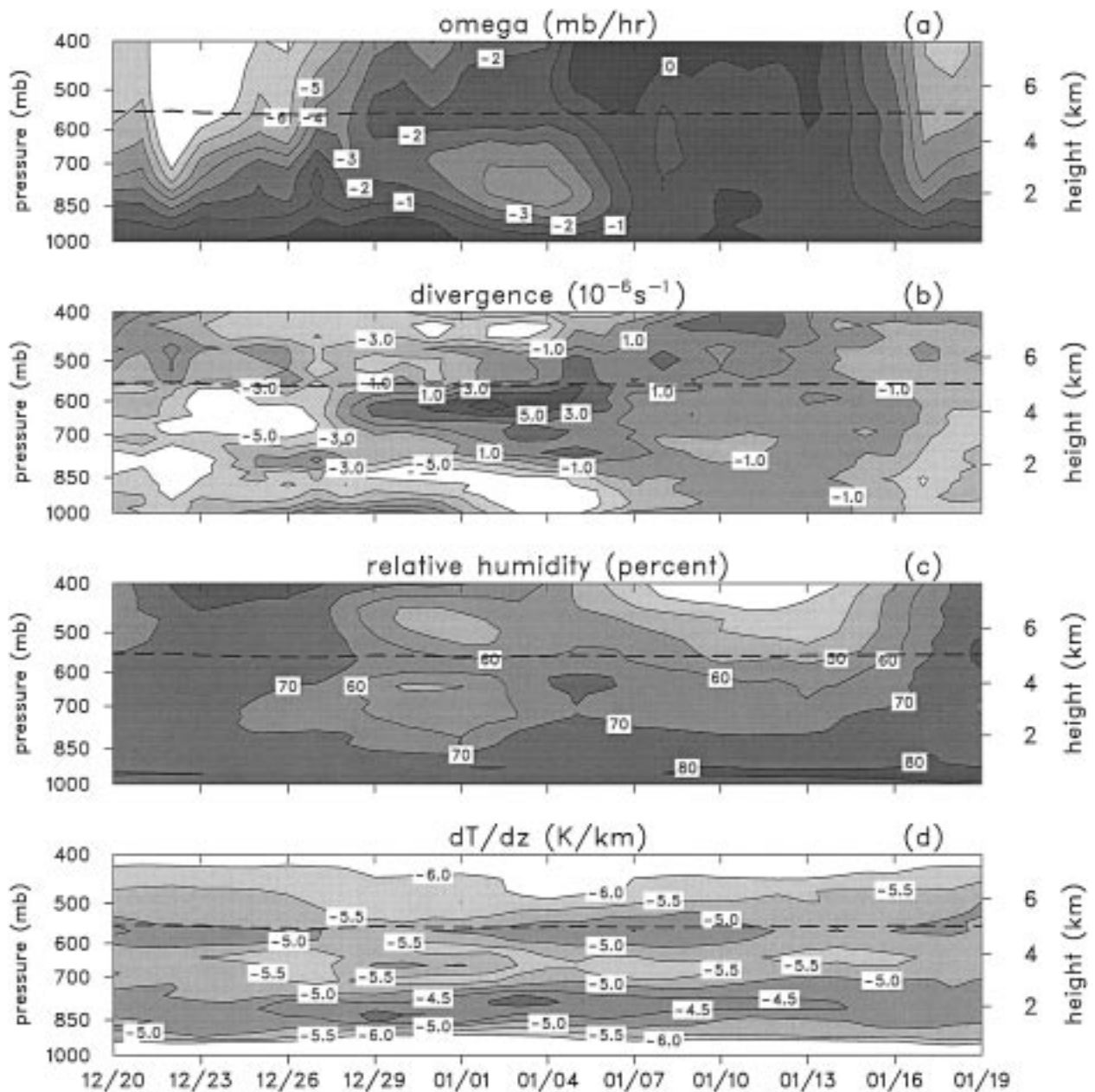
FIG. 12. As in Fig. 10 except for cruise 2 of R/V *Vickers.*

Lidar System aboard the NASA ER-2 aircraft (Spinhirne et al. 1996). Preliminary results indicate multiple cloud layers over the warm pool, but three layers stand out: one at the cirrus level (near the tropopause), one in the midtroposphere (5–8 km), and another between 2 and 3 km (J. Spinhirne 1997, personal communication).

A recently constructed climatology of the meridional wind at Christmas Island (2°N, 157°W) based on 50-MHz wind profiler measurements (Gage et al. 1997) reveals a midlevel divergence maximum outside the

Northern Hemisphere ITCZ at 5°–10°N. Gage et al. point out that satellite rainfall estimate studies indicate substantial warm-rain processes in the ITCZ near the longitudes of Christmas Island and that the midlevel divergence may be a signature of divergence from the numerous warm-rain (congestus) cells.

In a cloud-resolving numerical modeling study of the diurnal variation of deep convection in COARE, Liu and Moncrieff (1998) have reported a trimodal distribution of the fractional cloudiness, with peaks near 2, 6–7, and 13–14 km. Their results are consistent with
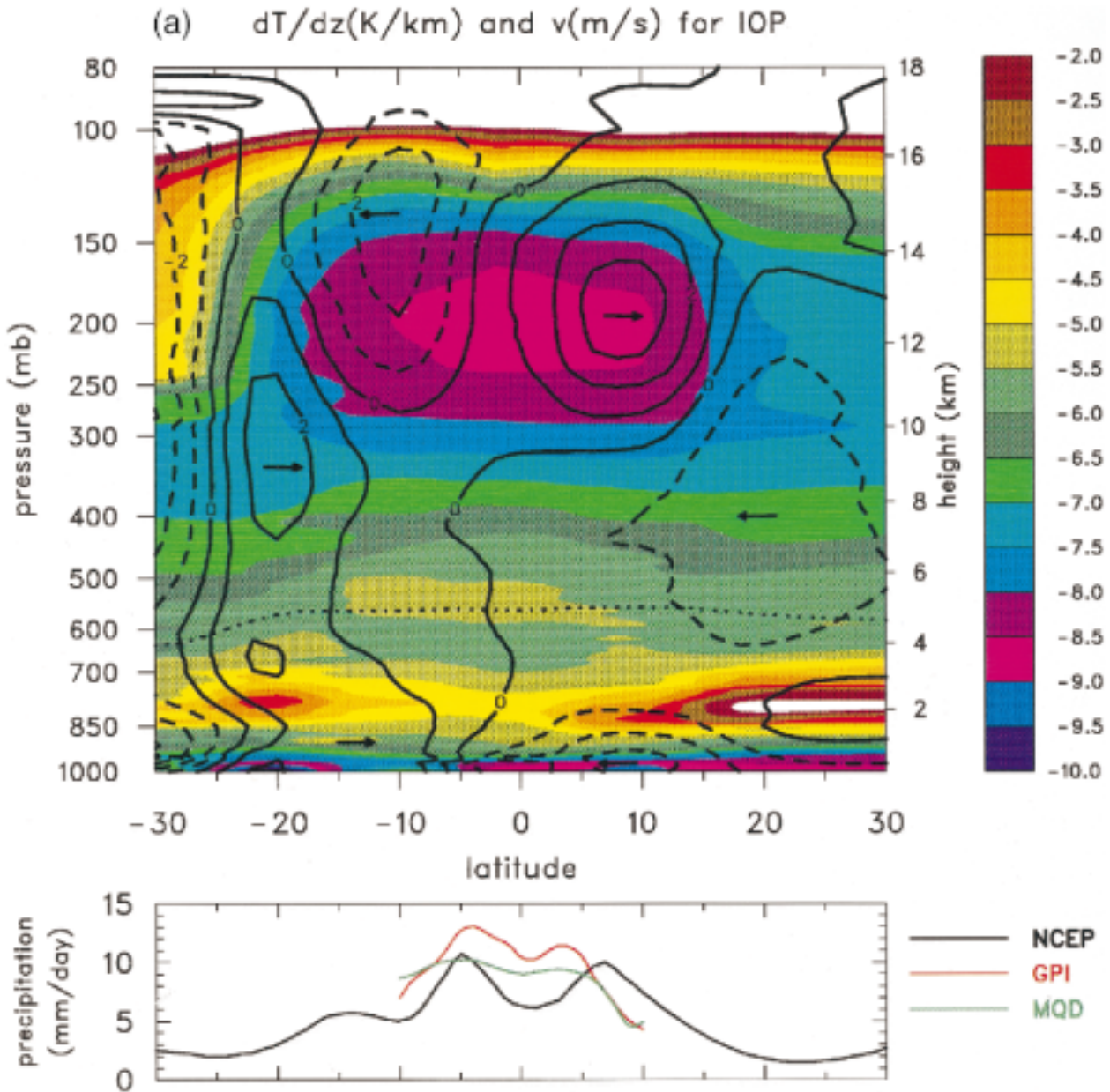
FIG. 13. (a) (upper) North–south cross section of COARE IOP-mean values of dT/dz in color (contour interval: 0.5 K km^{-1}; dashed line indicates 0°C level) and meridional wind (contour interval: 1 m s^{-1}). No colors are used for values of $dT/dz > -2$ K km^{-1}, which corresponds to the tropopause at the top of the figure. (lower) IOP-mean precipitation rates based on three techniques: NCEP reanalysis, GOES Precipitation Index (GPI), and multiquadric objective analysis (MQD). The latter two are computed only from 10°N to 10°S. (b) Conceptual model of tropical cumulus cloud distributions from 30°N to 30°S based on IOP-mean radar data and thermal stratification shown in (a). Three main

the trimodal distribution of detrainment shown in Fig. 6 (from Zuidema 1998).

5. Revised conceptual model of tropical clouds

The results of this study point to a revised picture of the distribution of tropical cumulus clouds and associated inversions and stable layers. To put the findings into proper context with COARE data, we first present

a north–south cross section of stability (dT/dz) and the mean meridional wind (v) from 30°N to 30°S within the longitude band centered over the IFA (150°–170°E) for the IOP (Fig. 13a). This cross section is based upon a gridded analysis of the sounding data within and surrounding the COARE domain at 2° horizontal and 10-mb vertical resolution (Ciesielski et al. 1997). As in Fig. 5, three stable layers are again evident, but there are important north–south variations in all of them. As ex-
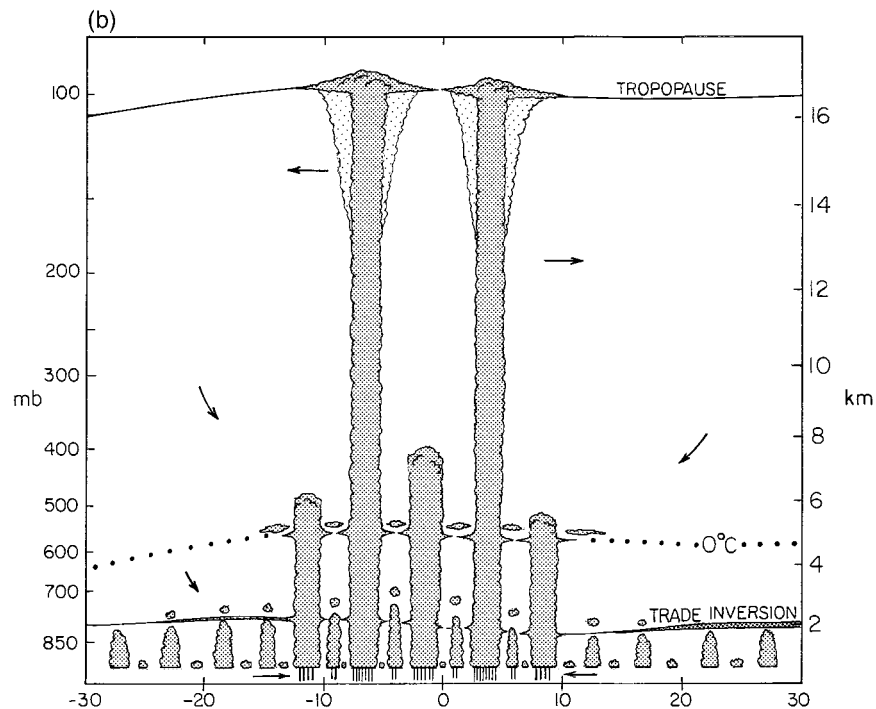
FIG. 13. (*Continued*) cloud types are indicated: shallow cumulus, cumulus congestus, and cumulonimbus. Within the shallow cumulus classification, there are two subdivisions: forced and active cumulus. Three stable layers are indicated: the trade inversion, the 0°C layer, and the tropopause. Shelf clouds and cloud debris near the trade and 0°C stable layers represent detrainment there. Cirrus anvils occur near the tropopause. Considerable overshooting of the trade and 0°C stable layers occurs in the equatorial trough zone. Arrows indicate meridional circulation. Although double ITCZ is indicated, representing IOP-mean, this structure is transient over the warm pool and a single ITCZ often exists.

pected, the trade inversion is strongest between 20° and 30° but still extends across the equator. The trade inversion is quasi-horizontal across the equator, consistent with the findings of Kloesel and Albrecht (1989) and Schubert et al. (1995). Actually, there appears to be a slight dip in the height of the inversion near the equator. This dip is consistent with the idea advanced by Schubert et al. (1995) that a dynamical adjustment and spreading of the inversion takes place along isentropes, which in the lower troposphere dip slightly downward across the equator (e.g., Fig. 7.6 of Peixoto and Oort 1992).

The 0°C stable layer is confined to the tropical latitudes, reflecting the fact that it is closely linked to deep convective activity and melting (Johnson et al. 1996). This connection can be seen by referring to the lower panel of Fig. 13a, where IOP-mean distributions of precipitation are presented based on three techniques: the National Centers for Environmental Prediction (NCEP) reanalysis (Kalnay et al. 1996), the Geostationary Operational Environmental Satellite (GOES) precipitation index (Arkin and Meisner 1987), and a budget-derived estimate based on a multiquadric objective analysis of sounding data (Ciesielski et al. 1997). All precipitation estimates suggest a double-ITCZ structure in the mean,

although the amplitudes and latitudes of the peaks vary somewhat from one technique to another. Also notable in Fig. 13a is a deep layer of steep lapse rates in the upper troposphere, which is collocated with deep equatorial convection. The tropopause has its maximum height near 100 mb or 16.5 km near the equator. Since COARE occurred during boreal winter, the position of the weakest trade stable layer, the center of the 0°C stable layer, the maximum rainfall, and the highest tropopause are shifted south of the equator. This shift is consistent with the mean meridional flow; that is, the v = 0 line at the surface and aloft is near 5°S. A peak in the divergent meridional flow occurs between 150 and 200 mb, with a primary maximum in convergent v at the surface and a secondary one between 300 and 400 mb.

Using the fields in Fig. 13a as a guide, a revised depiction of tropical cloud distributions is shown in Fig. 13b. The major revision from the conceptual model in Fig. 1 is the addition of a third cloud population, cumulus congestus. Numerous congestus clouds overshoot the 0°C stable layer by 1 to 2 km, but in many cases not sufficiently to glaciate. In instances where they do glaciate, they can have sufficient buoyancy to rise to the tropopause (Zuidema 1998). In addition, enhanced

detrainment from cumulonimbi can occur near 0°C because of the increased stability there (Bretherton and Smolarkiewicz 1989; Taylor and Baker; Raymond and Blyth 1992; Mapes and Zuidema 1996). This detrainment leads to enhanced cloud layers or shelf clouds near the 0°C level, which have been reported in the tropical western Pacific research flights of Malkus and Riehl (1964), are suggested in the relative humidity analyses of Mapes and Zuidema (1996) (their Fig. 18), and appear in the cloud-resolving modeling results of Liu and Moncrieff (1998). Since the cross section in Fig. 13a is in the western Pacific, stratocumulus regimes are not indicated in the poleward extremes of Fig. 13b. Also, for clarity, mesoscale convective systems, along with their associated stratiform precipitation regions (Houze 1977; Zipser 1977), have been omitted from Fig. 13b.

Figure 13b shows congestus clouds and the 0°C stable layers generally confined to the deep Tropics. These features vary temporally on the timescale of the 30–60-day oscillation, as discussed in section 3. The stable layer near the 0°C level is strongest at times of deep convective activity and MCS-scale organization (cf. Figs. 10d and 9, Figs. 12d and 11). This relationship is consistent with the idea that cooling by melting snow and ice is an important mechanism for the production of stable layers near the 0°C level (e.g., Findeisen 1940; Stewart et al. 1984; Willis and Heymsfield 1989). In other words, many of the stable layers during these periods may be the remnant effects of melting in preexisting convection (Johnson et al. 1996). The abundance of congestus clouds within the MCS category (Fig. 2), with a peak in echo tops at 7.5 km, may reflect the impact of stronger 0°C stable layers at these times. At other times the 0°C stable layer, present in a weaker form, may be related to the remote effects of convection, as suggested by Johnson et al. (1996) and Mapes and Zuidema (1996). One possibility is that, similar to the trade inversion, the 0°C stable layer can be dynamically extended into the deep Tropics from the ITCZ bands to the north and south. Results from computations using methods similar to those employed in Schubert et al. (1995), involving observed melting-induced cooling profiles within two relatively narrow zonal ITCZ bands at 10°N and S, show that after 3 days there is a remote effect in the cloud-free region along the equator, namely, an increase in stability of 1.5 C° km^{-1} near the 0°C level. Another possibility is that the stable layers are the result of gravity waves or "buoyancy bores" emanating from deep convection. Mapes (1993) and Mapes and Houze (1995) showed that the stratiform component to the heating produces a bore that moves away from the heat source at 20–25 m s^{-1} characterized by sinking motion aloft and rising motion at low levels, which leaves in its wake a layer of enhanced stability in the midtroposphere several hundred kilometers long. Finally, there is also the possibility that some of the 0°C stable layers are a reflection of radiative stabilization of dry intrusions in the midtroposphere that were com-

monplace over the warm pool (Mapes and Zuidema 1996).

Also depicted in Fig. 13b is a quasi-horizontal trade inversion in the subtropics transitioning to a stable layer in the Tropics, although its height is shown to decrease slightly near the equator. COARE observations suggest this behavior, although it is not clear how representative it is of the entire Tropics. An equatorward deepening of the trade wind layer between 30° and 15°, as depicted in Fig. 1, is not evident in this north–south section over the western Pacific (except, perhaps a slight deepening between 30° and 20°S). To some extent, the equatorward deepening in Fig. 1 (Simpson 1992) is intended to portray the structure along trade wind trajectories (e.g., Riehl et al. 1951; Malkus 1958), but the observations of Gutnick (1958) also show a north-to-south increase in the trade inversion depth over the western North Atlantic. Also, the results of von Ficker (1936) [also see Fig. 5.7 of Riehl 1979] in the eastern Atlantic show the height of the trade inversion base increasing all the way to the equator. Apparently, this behavior is not characteristic of the western Pacific, at least during the period of COARE.

As the trade stable layer weakens equatorward, overshooting of this layer by shallow cumuli [indicated by detached cloud elements above the layer, following Malkus (1954, 1958)] progressively increases toward the equator (note peak in sub-MCS echo heights at 3.5 km in Fig. 2). In addition, two types of shallow, trade cumuli are indicated: one very shallow or forced, representing overshooting, mechanically driven boundary layer eddies; and the other deeper or active, where latent heating plays an important role in their evolution (Esbensen 1978; Randall 1980; Stull 1985; Johnson and Lin 1997). Also, Malkus and Riehl (1964) report numerous cloud shelves near 2–2.5 km attached to congestus and cumulonimbus clouds in the tropical western Pacific, which are illustrated in Fig. 13b.

The cloud distributions shown in Fig. 13b are based on IOP-mean fields. The two tall towers are positioned at the approximate latitudes of maximum IOP-mean upward motion (Lin and Johnson 1996a) and precipitation (Fig. 13a). We caution that this pattern is not representative of all times during the IOP: variations to it occured with regularity.

6. Summary and conclusions

Observations from the recent TOGA COARE have provided new evidence concerning the distribution of tropical clouds. Cumulus echo-top statistics from the 5-cm radar aboard the R/V *Vickers* indicate that *cumulus congestus* clouds are the most abundant of all *precipitating* clouds in COARE. Specifically, congestus with tops between 4.5 and 9.5 km represent 57% of the precipitating convective clouds in COARE. Radar studies from GATE reveal a similar result. When combined with photographic estimates of the *nonprecipitating* cumulus

population, it is suggested that the overall cumulus cloud distribution is bimodal, abundant shallow cumulus and cumulus congestus. But these are not the two modes that are often argued to be present based on studies of cloud-base mass fluxes, detrainment, etc., namely, shallow and deep clouds. Therefore, we have conflicting views: radar and photographic data show shallow cumulus and congestus clouds to be the most abundant types, but other studies (budgets, etc.) have led to conceptual models that emphasize shallow cumuli and cumulonimbi (e.g., Fig. 1) as the two prominent cloud types. The point we want to make in the paper is that all *three* cloud types—cumulus, congestus, and cumulonimbus—are important components of the tropical convective cloud spectrum. Also, these cloud types are associated with trimodal distributions of divergence, cloud detrainment, and fractional cloudiness in the Tropics.

The peaks in the distributions of these three cloud types are in close proximity to prominent stable layers that exist over the Pacific warm pool and the tropical eastern Atlantic: near 2 km (the trade stable layer), ~5 km (near 0°C), and ~15–16 km (the tropopause). These stable layers serve to inhibit cloud growth and promote cloud detrainment. Capping of cloud growth, with some overshooting, is well known for the trade stable layer and tropopause. However, it is less well known for the 0°C stable layer. But recent cloud modeling studies (e.g., Zuidema 1998) indicate that while the stable layer near the 0°C level is relatively weak, it can contribute to an enhancement of detrainment just above it (near 7.5 km or 400 mb) for those congestus clouds that do not glaciate (evidently a common occurrence over the warm pool). The existence of a peak in the frequency distribution of echo tops near this level at times of organization of convection on the MCS ($\geq$100 km)scale suggests that processes that contribute to enhanced detrainment near that level may also contribute to restricting cloud growth to that level. While vigorous, undilute updrafts in cumulonimbi are not stopped by the 0°C stable layers, many congestus clouds over the warm pool are heavily loaded with precipitation and strongly entraining, such that the increased stability near 0°C can inhibit cloud growth. This assertion is supported by other COARE radar studies (Uyeda et al. 1995; Hildebrand 1998), which report a close association between the 0°C level and the vertical structure and growth of convection over the warm pool. It is also supported by recent cloud-resolving modeling experiments showing a trimodal distribution of fractional cloudiness over the warm pool, with peaks near 2, 6–7, and 13–14 km (Liu and Moncrieff 1998).

Evidence of enhanced detrainment near the trade and 0°C stable layers can also be found in the cloud photographic analyses of Malkus and Riehl (1964) and in much more recent aircraft lidar measurements, which indicate frequent cloud layers near these two levels, as well as the tropopause. It is plausible that the 0°C-level detrainment may produce many of the midlevel clouds in the Tropics, thereby modulating the radiative heating of the tropical atmosphere.

The three cloud populations are found to vary significantly on the timescale of the 30–60-day intraseasonal oscillation. During mid to late November and early December of TOGA COARE the frequency of cumulus and congestus clouds increased as seen by the MIT radar aboard the R/V *Vickers* as the SST rose. Correspondingly, there was a deepening of the moist layer in the lower troposphere in the presence of large-scale subsidence. The increasing shallow and midlevel echo populations played an important role in preconditioning the atmosphere for deep convection that occurred in mid-December just prior to the strongest of the COARE westerly wind bursts. In late December and early January, as the SST decreased due to high winds, increased evaporation, ocean mixing, and increased cloudiness, the number of deep echoes and shallow, precipitating cumuli decreased to nearly zero. However, nonprecipitating shallow cumuli, particularly those of the forced type representing overshooting boundary layer eddies, were abundant during the westerly wind bursts (Johnson and Lin 1997). Then, as the SST rose again toward mid-January, the numbers of precipitating cumulus and congestus clouds increased and a remoistening of the lower troposphere occurred.

Although the cumulus congestus clouds are not as heavily raining as their deep cumulonimbus counterparts, they do produce a substantial fraction of the total rainfall over the warm pool. Congestus with tops below 10 km contribute 28% of total convective rainfall in COARE. For the sub-MCS category (cloud systems having contiguous precipitation echoes <100 km in horizontal scale), the fraction is even greater, 52%, or over half the total convective rainfall of that category. In other words, many of the isolated cells in COARE are of the congestus cloud variety, which often produce heavy rain, presumably in part due to the effective warm-rain processes over the exceptionally warm ocean in this part of the world. Of course, ice processes are important for the deeper portion of the congestus cloud spectrum.

While evidence has been presented from COARE and GATE concerning the importance of three convective cloud types—cumulus, congestus, and cumulonimbus—further work is needed to understand the nature of each of these cloud types and their dynamical, hydrological, and radiative significance. What factors determine the relative abundance of the three cloud types in different atmospheric regimes? Do they vary on seasonal, annual, and interannual [El Niño–Southern Oscillation (ENSO)] timescales? To what extent do shallow cumulus and congestus clouds detrain near the trade and 0°C stable layers, respectively, and contribute to debris and layer clouds at those levels? What are the subsequent impacts on the atmospheric water vapor and radiative fields? How sensitive are the ultimate heights of congestus

clouds to glaciation and at what levels do congestus clouds in the Tropics typically glaciate? How do the radar results in this study, which pertain to precipitation-sized particles, compare to satellite-based estimates of cloud populations, which pertain to cloud-sized particles often covering much larger areas? It is hoped that these and other questions can be addressed with data from COARE, future field programs on tropical convection, and cloud modeling efforts.

REFERENCES

Agee, E. M., 1984: Observations from space and thermal convection: A historical perspective. *Bull. Amer. Meteor. Soc.,* **65,** 938–949.

Albrecht, B. A., 1984: A model of the study of the downstream variations of the thermodynamic structure of the trade winds. *Tellus,* **36A,** 187–202.

——, A. K. Betts, W. H. Schubert, and S. K. Cox, 1979: A model of the thermodynamic structure of the trade-wind boundary layer: Part I. Theoretical formulation and sensitivity tests. *J. Atmos. Sci.,* **36,** 73–89.

Arkin, P. A., and B. N. Meisner, 1987: The relationship between large-scale convective rainfall and cold cloud over the western hemisphere during 1982–1984. *Mon. Wea. Rev.,* **115,** 51–74.

Augstein, E., H. Riehl, F. Ostapoff, and V. Wagner, 1973: Mass and energy transports in an undisturbed Atlantic trade-wind flow. *Mon. Wea. Rev.,* **101,** 101–111.

Betts, A. K., 1973: Nonprecipitating cumulus convection and its parameterization. *Quart. J. Roy. Meteor. Soc.,* **99,** 178–196.

——, 1975: Parametric interpretation of trade-wind cumulus budget studies. *J. Atmos. Sci.,* **32,** 1934–1945.

——, 1982: Saturation point analysis of moist convective overturning. *J. Atmos. Sci.,* **39,** 1484–1505.

——, and W. Ridgway, 1988: Coupling of the radiative, convective, and surface fluxes of the equatorial Pacific. *J. Atmos. Sci.,* **45,** 522–536.

Bretherton, C. S., 1993: Understanding Albrecht's model of trade cumulus cloud fields. *J. Atmos. Sci.,* **50,** 2264–2283.

——, and P. K. Smolarkiewicz, 1989: Gravity waves, compensating subsidence and detrainment around cumulus clouds. *J. Atmos. Sci.,* **46,** 740–759.

Cheng, C.-P., and R. A. Houze Jr., 1979: The distribution of convective and mesoscale precipitation in GATE radar echo patterns. *Mon. Wea. Rev.,* **107,** 1370–1381.

Cheng, M.-D., 1989: Effects of downdrafts and mesoscale convective organization on the heat and moisture budgets of tropical cloud clusters. Part II: Effects of convective-scale downdrafts. *J. Atmos. Sci.,* **46,** 1540–1564.

Ciesielski, P. E., L. M. Hartten, and R. H. Johnson, 1997: Impacts of merging profiler and rawinsonde winds on TOGA COARE analyses. *J. Atmos. Oceanic Technol.,* **14,** 1264–1279.

DeMott, C. A., and S. A. Rutledge, 1998a: The vertical structure of TOGA COARE convection. Part I: Radar echo distributions. *J. Atmos. Sci.,* **55,** 2730–2747.

——, and ——, 1998b: The vertical structure of TOGA COARE

convection. Part II: Modulating influences and implications for diabatic heating *J. Atmos. Sci.,* **55,** 2748–2762.

Emanuel, K. A., 1994: *Atmospheric Convection.* Oxford University Press, 580 pp.

Esbensen, S., 1978: Bulk thermodynamic effects and properties of small tropical cumuli. *J. Atmos. Sci.,* **35,** 826–837.

——, E. I. Tollerud, and J.-H. Chu, 1982: Cloud-cluster-scale circulations and the vorticity budget of synoptic-scale waves over the eastern Atlantic intertropical convergence zone. *Mon. Wea. Rev.,* **110,** 1677–1692.

Findeisen, W., 1940: The formation of the 0°C isothermal layer and fractocumulus under nimbostratus. *Meteor. Z.,* **57,** 49–54.

Firestone, J. K., and B. A. Albrecht, 1986: The structure of the atmospheric boundary layer in the central equatorial Pacific during January and February of FGGE. *Mon. Wea. Rev.,* **114,** 2219–2231.

Gage, K. S., G. N. Kiladis, L. M. Hartten, and C. R. Williams, 1997: A ten-year climatology of meridional winds over the central equatorial Pacific utilizing the Christmas Island wind profiler: Annual cycle and vertical structure. Preprints, *22d Conf. on Hurricanes and Tropical Meteorology,* Fort Collins, CO, Amer. Meteor. Soc., 501–502.

Godfrey, J. S., R. A. Houze Jr., R. H. Johnson, R. Lukas, J.-L. Redelsperger, A. Sumi, and R. Weller, 1998: The Coupled Ocean Atmosphere Response Experiment (COARE): An interim report. *J. Geophys. Res.,* **103,** 14 395–14 450.

Gutnick, M., 1958: Climatology of the trade-wind inversion in the Caribbean. *Bull. Amer. Meteor. Soc.,* **39,** 410–420.

Gutzler, D. S., G. N. Kiladis, G. A. Meehl, K. M. Weickmann, and M. Wheeler, 1994: The global climate of December 1992–February 1993. Part II: Large-scale variability across the tropical western Pacific during TOGA COARE. *J. Climate,* **7,** 1606–1622.

Hildebrand, P. H., 1998: Shear-parallel moist convection over the tropical ocean: A case study from 18 February 1993 TOGA COARE. *Mon. Wea. Rev.,* **126,** 1952–1976.

Holland, J. Z., and E. M. Rasmusson, 1973: Measurements of the atmospheric mass, energy and momentum budgets over a 500-kilometer square of tropical ocean. *Mon. Wea. Rev.,* **101,** 44–55.

Holle, R. L., J. Simpson, and S. W. Leavitt, 1979: GATE B-scale cloudiness from whole-sky cameras on four U.S. ships. *Mon. Wea. Rev.,* **107,** 874–895.

Houze, R. A., Jr., 1977: Structure and dynamics of a tropical squall-line system observed during GATE. *Mon. Wea. Rev.,* **105,** 1540–1567.

——, 1993: *Cloud Dynamics.* Academic Press, 573 pp.

——, and C.-P. Cheng, 1977: Radar characteristics of tropical convection observed during GATE: Mean properties and trends over the summer season. *Mon. Wea. Rev.,* **105,** 964–980.

——, and A. K. Betts, 1981: Convection in GATE. *Rev. Geophys. Space Phys.,* **19,** 541–576.

Johnson, R. H., 1976: The role of convective-scale precipitation downdrafts in cumulus and synoptic-scale interactions. *J. Atmos. Sci.,* **33,** 1890–1910.

——, 1980: Diagnosis of convective and mesoscale motions during Phase III of GATE. *J. Atmos. Sci.,* **37,** 733–753.

——, and X. Lin, 1997: Episodic trade wind regimes over the western Pacific warm pool. *J. Atmos. Sci.,* **54,** 2020–2034.

——, P. E. Ciesielski, and K. A. Hart, 1996: Tropical inversions near the 0°C level. *J. Atmos. Sci.,* **53,** 1838–1855.

Kalnay, E., and Coauthors, 1996: The NCEP/NCAR 40-Year Reanalysis Project. *Bull. Amer. Meteor. Soc.,* **77,** 437–471.

Kingsmill, D. E., and R. M. Wakimoto, 1991: Kinematic, dynamic, and thermodynamic analyses of a weakly sheared severe thunderstorm over northern Alabama. *Mon. Wea. Rev.,* **119,** 262–297.

Kloesel, K. A., and B. A. Albrecht, 1989: Low-level inversions over the tropical Pacific—Thermodynamic structure of the boundary

layer and above-inversion moisture structure. *Mon. Wea. Rev.,* **117,** 87–101.

Krueger, A. F., and S. Fritz, 1961: Cellular cloud patterns revealed by TIROS I. *Tellus,* **13,** 1–7.

Kuettner, J. P., 1959: The band structure of the atmosphere. *Tellus,* **11,** 267–294.

——, 1971: Cloud bands in the earth's atmosphere. Observations and theory. *Tellus,* **23,** 404–425.

Lau, K.-M., and C.-H. Sui, 1997: Mechanisms of short-term sea surface temperaure regulation: Observations during TOGA COARE. *J. Climate,* **10,** 465–472.

Leary, C. A., and R. A. Houze Jr., 1979: The structure and evolution of convection in a tropical cloud cluster. *J. Atmos. Sci.,* **36,** 437–457.

LeMone, M. A., and R. J. Meitin, 1984: Three examples of fair-weather mesoscale boundary layer convection in the Tropics. *Mon. Wea. Rev.,* **112,** 1985–1997.

Lin, X., and R. H. Johnson, 1996a: Kinematic and thermodynamic characteristics of the flow over the western Pacific warm pool during TOGA COARE. *J. Atmos. Sci.,* **53,** 695–715.

——, and ——, 1996b: Heating, moistening, and rainfall over the western Pacific warm pool during TOGA COARE. *J. Atmos. Sci.,* **53,** 3367–3383.

Liu, C., and M. W. Moncrieff, 1998: A numerical study of the diurnal cycle of tropical oceanic convection. *J. Atmos. Sci.,* **55,** 2329–2344.

López, R. E., 1976: Radar characteristics of cloud populations of tropical disturbances in the northwest Atlantic. *Mon. Wea. Rev.,* **104,** 268–283.

——, 1977: The lognormal distribution and cumulus cloud populations. *Mon. Wea. Rev.,* **105,** 865–872.

——, 1978: Internal structure and development processes of C-scale aggregates of cumulus clouds. *Mon. Wea. Rev.,* **106,** 1488–1494.

Malkus, J. S., 1954: Some results of a trade-cumulus cloud investigation. *J. Meteor.,* **11,** 220–237.

——, 1958: On the structure of the trade-wind moist layer. Papers on Physical Oceanography and Meteorology, Vol. 13, No. 2, Massachusetts Institute of Technology and Woods Hole Oceanographic Institute, 47 pp. [Available from Dr. Joanne Simpson, Earth Scienes Directorate, Mail Code 912, Goddard Space Flight Center/NASA, Greenbelt, MD 20771.]

——, 1962: Large-scale interactions. *The Sea: Ideas and Observations on Progress in the Study of the Seas,* John Wiley and Sons, 88–294.

——, and H. Riehl, 1964: *Cloud Structure and Distributions over the Tropical Pacific Ocean.* University of California Press, 229 pp.

Mapes, B. E., 1993: Gregarious tropical convection. *J. Atmos. Sci.,* **50,** 2026–2037.

——, and R. A. Houze Jr., 1995: Diabatic divergence profiles in western Pacific mesoscale convective systems. *J. Atmos. Sci.,* **52,** 1807–1828.

——, and P. Zuidema, 1996: Radiative-dynamical consequences of dry tongues in the tropical atmosphere. *J. Atmos. Sci.,* **53,** 620–638.

McGuffie, K., and A. Henderson-Sellers, 1989: Almost a century of "imaging" clouds over the whole-sky dome. *Bull. Amer. Meteor. Soc.,* **70,** 1243–1253.

Neiburger, M., 1960: The relation of air mass structure to the field of motion over the eastern North Pacific Ocean in summer. *Tellus,* **12,** 31–40.

——, D. S. Johnson, and C. W. Chien, 1961: *Studies of the Structure of the Atmosphere over the Eastern Pacific Ocean in Summer. I: The Inversion over the Eastern North Pacific Ocean.* University of California Press, 94 pp.

Newell, R. E., and Coauthors, 1996: Vertical fine-scale atmospheric structure measured from NASA DC-8 during PEM-West A. *J. Geophys. Res.,* **101,** 1943–1960.

Nicholls, S., and M. A. LeMone, 1980: Fairweather boundary layer in GATE: The relationship of sublcoud fluxes and structure to

the distribution and enhancement of cumulus clouds. *J. Atmos. Sci.,* **37,** 2051–2067.

Nitta, T., 1972: Energy budget of wave disturbances over the Marshall Islands during the years of 1956 and 1958. *J. Meteor. Soc. Japan,* **50,** 71–84.

——, 1978: A diagnostic study of interaction of cumulus updrafts and downdrafts with large-scale motions in GATE. *J. Meteor. Soc. Japan,* **56,** 232–242.

——, and S. Esbensen, 1974: Heat and moisture budget analyses using BOMEX data. *Mon. Wea. Rev.,* **102,** 17–28.

Numaguti, A., R. Oki, K. Nakamura, K. Tsuboki, N. Misawa, T. Asai, and Y.-M. Kodama, 1995: 4–5-day-period variations and low-level dry air observed in the equatorial western Pacific during the TOGA-COARE IOP. *J. Meteor. Soc. Japan,* **73,** 267–290.

Ogura, Y., and H.-R. Cho, 1973: Diagnostic determination of cumulus populations from large-scale variables. *J. Atmos. Sci.,* **30,** 1276–1286.

Ooyama, K. V., 1987: Scale-controlled objective analysis. *Mon. Wea. Rev.,* **115,** 2479–2506.

Parsons, D., and Coauthors, 1994: The Integrated Sounding System: Description and preliminary observations from TOGA COARE. *Bull. Amer. Meteor. Soc.,* **75,** 553–567.

Peixoto, J. P., and A. H. Oort, 1992: *Physics of Climate.* American Institute of Physics, 520 pp.

Platt, C. M. R., D. M. Winker, and M. A. Vaughan, 1999: Backscatter-to-extinction ratios in the top layers of tropical mesoscale convective sytems and in isolated cirrus from LITE observations. *J. Appl. Meteor.,* in press.

Randall, D. A., 1980: Conditional instability of the first kind upside-down. *J. Atmos. Sci.,* **37,** 125–130.

Raymond, D. J., and A. M. Blyth, 1992: Extension of the stochastic mixing model to cumulonimbus clouds. *J. Atmos. Sci.,* **49,** 1968–1983.

——, R. Solomon, and A. M. Blyth, 1991: Mass fluxes in New Mexico mountain thunderstorms from radar and aircraft measurements. *Quart. J. Roy. Meteor. Soc.,* **117,** 587–621.

Reed, R. J., and E. E. Recker, 1971: Structure and properties of synoptic-scale wave disturbances in the equatorial western Pacific. *J. Atmos. Sci.,* **28,** 1117–1133.

Rickenbach, T. M., and S. A. Rutledge, 1997: The diurnal variation of rainfall over the western Pacific warm pool: Dependence on convective organization. Preprints, *22d Conf. on Hurricanes and Tropical Meteorology,* Fort Collins, CO, Amer. Meteor. Soc., 205–206.

——, and ——, 1998: Convection in TOGA COARE: Horizontal scale, morphology, and rainfall production. *J. Atmos. Sci.,* **55,** 2715–2729.

Riehl, H., 1979: *Climate and Weather in the Tropics.* Academic Press, 611 pp.

——, and J. S. Malkus, 1958: On the heat balance in the equatorial trough zone. *Geophysica,* **6,** 503–538.

——, and J. Simpson, 1979: The heat balance of the equatorial trough zone, revisited. *Contrib. Atmos. Phys.,* **52,** 287–304.

——, T. C. Yeh, J. S. Malkus, and N. E. LaSeur, 1951: The northeast trade of the Pacific Ocean. *Quart. J. Roy. Meteor. Soc.,* **77,** 598–626.

Rutledge, S. A., and Coauthors, 1993: The shipboard deployment of the MIT C-band radar during TOGA COARE. Preprints, *26th Int. Conf. on Radar Meteorology,* Norman, OK, Amer. Meteor. Soc., 371–373.

Sarachik, E. S., 1985: A simple theory for the vertical structure of the tropical atmosphere. *Pure Appl. Geophys.,* **123,** 261–271.

Schubert, W. H., 1976: Experiments with Lilly's cloud-topped mixed layer model. *J. Atmos. Sci.,* **33,** 436–446.

——, J. S. Wakefield, E. J. Steiner, and S. K. Cox, 1979a: Marine stratocumulus convection. Part I: Governing equations and horizontally homogeneous solutions. *J. Atmos. Sci.,* **36,** 1286–1307.

——, ——, ——, and ——, 1979b: Marine stratocumulus convection. Part II: Horizontally inhomogeneous solutions. *J. Atmos. Sci.,* **36,** 1308–1324.

——, P. E. Ciesielski, C. Lu, and R. H. Johnson, 1995: Dynamical adjustment of the trade wind inversion layer. *J. Atmos. Sci.,* **52,** 2941–2952.

Simpson, J., 1992: Global circulation and tropical cloud activity. *The Global Role of Tropical Rainfall,* J. S. Theon et al., Eds., A. Deepak Publishing, 77–92.

Soloviev, A., and R. Lukas, 1997: Observation of large diurnal warming events in the near-surface layer of the western Pacific warm pool. *Deep-Sea Res.,* **44,** 1055–1076.

Spinhirne, J. D., W. D. Hart, and D. L. Hlavka, 1996: Cirrus infrared parameters and shortwave reflectance relations from observations. *J. Atmos. Sci.,* **53,** 1438–1458.

Steiner, M., R. A. Houze Jr., and S. E. Yuter, 1995: Climatological characteristics of three-dimensional storm structure from operational radar and rain gauge data. *J. Appl. Meteor.,* **34,** 1978–2007.

Stewart, R. E., J. D. Marwitz, J. C. Pace, and R. E. Carbone, 1984: Characteristics through the melting layer of stratiform clouds. *J. Atmos. Sci.,* **41,** 3227–3237.

Stull, R. B., 1985: A fair-weather cumulus cloud classification scheme for mixed-layer studies. *J. Climate Appl. Meteor.,* **24,** 49–56.

Sui, C.-H., K.-M. Lau, Y. N. Takayabu, and D. A. Short, 1997: Diurnal variations in tropical oceanic cumulus convection during TOGA COARE. *J. Atmos. Sci.,* **54,** 639–655.

Sun, D.-Z., and R. S. Lindzen, 1993: Distribution of tropical tropospheric water vapor. *J. Atmos. Sci.,* **50,** 1643–1660.

Taylor, G. R., and M. B. Baker, 1991: Entrainment and detrainment in cumulus clouds. *J. Atmos. Sci.,* **48,** 112–121.

Thompson, R. M., Jr., S. W. Payne, E. E. Recker, and R. J. Reed, 1979: Structure and properties of synoptic-scale wave disturbances in the intertropical convergence zone of the eastern Atlantic. *J. Atmos. Sci.,* **36,** 53–72.

Uyeda, H., and Coauthors, 1995: Doppler radar observations on the structure and characteristics of tropical clouds during the TOGA-COARE IOP in Manus, Papua New Guinea—Outline of the observation. *J. Meteor. Soc. Japan,* **73,** 415–425.

von Ficker, H., 1936: Die passatinversion. *Veroeff. Meteor. Inst. Univ. Berlin,* **1,** 1–33.

Wakefield, J. S., and W. H. Schubert, 1981: Mixed-layer model simulation of eastern North Pacific stratocumulus. *Mon. Wea. Rev.,* **109,** 1959–1968.

Warner, C., and G. L. Austin, 1978: Statistics of radar echoes on day 261 of GATE. *Mon. Wea. Rev.,* **106,** 983–994.

——, J. Simpson, G. Van Helvoirt, D. W. Martin, D. Suchman, and G. L. Austin, 1980: Deep convection on day 261 of GATE. *Mon. Wea. Rev.,* **108,** 169–194.

Webster, P. J., and R. Lukas, 1992: TOGA COARE: The Coupled Ocean–Atmosphere Response Experiment. *Bull. Amer. Meteor. Soc.,* **73,** 1377–1416.

Weller, R. A., and S. P. Anderson, 1996: Surface meteorology and air–sea fluxes in the western equatorial Pacific during the TOGA Coupled Ocean–Atmosphere Response Experiment. *J. Climate,* **9,** 1959–1990.

Williams, A. G., H. Kraus, and J. M. Hacker, 1996: Transport processes in the tropical warm pool boundary layer. Part I: Spectral composition of fluxes. *J. Atmos. Sci.,* **53,** 1187–1202.

Willis, P. T., and A. J. Heymsfield, 1989: Structure of the melting layer in mesoscale convective system stratiform precipitation. *J. Atmos. Sci.,* **46,** 2008–2025.

WMO, 1956: *International Cloud Atlas.* World Meteorological Organization, 155 pp.

Woodcock, A. H., 1940: Convection and soaring over the open sea. *J. Mar. Res.,* **3,** 248–253.

Xu, K., and K. A. Emanuel, 1989: Is the tropical atmosphere conditionally unstable? *Mon. Wea. Rev.,* **117,** 1471–1479.

Yanai, M., S. Esbensen, and J. H. Chu, 1973: Determination of bulk properties of tropical cloud clusters from large-scale heat and moisture budgets. *J. Atmos. Sci.,* **30,** 611–627.

——, J.-H. Chu, T. E. Stark, and T. Nitta, 1976: Response of deep and shallow tropical maritime cumuli to large-scale processes. *J. Atmos. Sci.,* **33,** 976–991.

Yoneyama, K., and T. Fujitani, 1995: The behavior of dry westerly air associated with convection observed during TOGA-COARE R/V *Natsushima* cruise. *J. Meteor. Soc. Japan,* **73,** 291–304.

Zipser, E. J., 1969: The role of organized unsaturated downdrafts in the structure and rapid decay of an equatorial disturbance. *J. Appl. Meteor.,* **8,** 799–814.

——, 1977: Mesoscale and convective-scale downdrafts as distinct components of squall-line circulation. *Mon. Wea. Rev.,* **105,** 1568–1589.

Zuidema, P., 1998: On the 600–800 mb minimum in tropical cloudiness. *J. Atmos. Sci.,* **55,** 2220–2228.